Inorganic Chemistry

Article

pubs.acs.org/IC

Photophysical and Photochemical Trends in Tricarbonyl Rhenium(I) N-Heterocyclic Carbene Complexes

Jamila G. Vaughan,[†] Brodie L. Reid,[†] Phillip J. Wright,[†] Sushil Ramchandani,[†] Brian W. Skelton,[‡] Paolo Raiteri,[†] Sara Muzzioli,[§] David H. Brown,[†] Stefano Stagni,*[,§] and Massimiliano Massi*[,†]

[†]Nanochemistry Research Institute, Department of Chemistry, Curtin University, Kent Street, Bentley 6102 Western Australia, Australia

[‡]Centre for Microscopy, Characterisation and Analysis, University of Western Australia, Crawley 6009 Western Australia, Australia

[§]Department of Industrial Chemistry "Toso Montanari", University of Bologna, viale del Risorgimento 4, Bologna 40126, Italy

Supporting Information

ABSTRACT: A family of tricarbonyl Re(I) complexes of the formulation *fac*-[Re(CO)$_3$(NHC)L] has been synthesized and characterized, both spectroscopically and structurally. The NHC ligand represents a bidentate N-heterocyclic carbene species where the central imidazole ring is substituted at the N3 atom by a butyl, a phenyl, or a mesityl group and substituted at the N1 atom by a pyridyl, a pyrimidyl, or a quinoxyl group. On the other hand, the ancillary L ligand alternates between chloro and bromo. For the majority of the complexes, the photophysical properties suggest emission from the lowest triplet metal-to-ligand charge transfer states, which are found partially mixed with triplet ligand-to-ligand charge transfer character. The nature and relative energy of the emitting states appear to be mainly influenced by the identity of the substituent on the N3 atom of the imidazole ring; thus, the pyridyl complexes have blue-shifted emission in comparison to the more electron deficient pyrimidyl complexes. The quinoxyl complexes show an unexpected blue-shifted emission, possibly occurring from ligand-centered excited states. No significant variations were found upon changing the substituent on the imidazole N3 atom and/or the ancillary ligand. The photochemical properties of the complexes have also been investigated, with only the complexes bound to the pyridyl-substituted NHC ligands showing photoinduced CO dissociation upon excitation at 370 nm, as demonstrated by the change in the IR and NMR spectra as well as a red shift in the emission profile after photolysis. Temperature-dependent photochemical experiments show that CO dissociation occurs at temperatures as low as 233 K, suggesting that the Re−C bond cleaves from excited states of metal-to-ligand charge transfer nature rather than thermally activated ligand field excited states. A photochemical mechanism that takes into account the reactivity of the complexes bound to the pyridyl-NHC ligand as well as the stability of those bound to the pyrimidyl- and quinoxyl-NHC ligands is proposed.

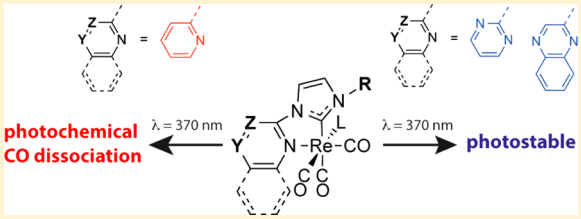

INTRODUCTION

The photophysical properties of luminescent tricarbonyl Re(I) complexes bound to π-conjugated ligands have been extensively studied. The general formulation of this class of compounds is *fac*-[Re(CO)$_3$(diim)L]$^{0/+}$, where diim represents a diimine ligand possessing a π^* system of accessible energy and L either an anionic or neutral monodentate ancillary ligand.[1] The most common diim ligands investigated are designed around 1,10-phenanthroline (phen) and 2,2′-bipyridine (bipy): it has been well established how chemical variations of these systems can be exploited to tune the photophysical properties of the Re complexes.[1] Coupled with favorable quantum yields, relatively long-lived excited state lifetimes, and resistance to photobleaching, the ability to tune the photophysical properties has made this class of complexes amenable for a variety of applied fields, ranging from organic light emitting devices (OLEDs) to cellular labels.[2−8]

In comparison to Re complexes bound to diim ligands, the analogous *fac*-[Re(CO)$_3$(NHC)L] complexes, where NHC represents a bidentate N-heterocyclic carbene ligand possessing an imine-type N atom and a carbene-type C atom as donors, have received considerably less attention. This is somewhat surprising, as NHC-type ligands have been extensively used to improve the luminescent properties in complexes of Ru(II), Ir(III), Pt(II), and Au(I).[9−13] With the intent to investigate the effect that the exchange of a diim for a NHC ligand would have on the luminescent properties of tricarbonyl Re complexes, our group and others have investigated the photophysical behavior of this class of compounds, where the NHC ligand is based around a pyridyl-, pyrimidyl-, or quinolyl-substituted imidazole or benzimidazole ring.[14−16] The findings have revealed that these types of NHC ligands are able to activate tunable metal-to-ligand charge transfer (MLCT) transitions through their π^* system, upon which phosphorescent decay to the ground state (GS) is then observed (^{3}MLCT → GS). These types of neutral

Received: December 24, 2013
Published: March 25, 2014

   dx.doi.org/10.1021/ic403138a | Inorg. Chem. 2014, 53, 3629−3641

complexes have highlighted a blue-shifted emission in comparison to their analogues bound to phen and bipy, with the blue shift being ascribed to a decrease in the overall conjugation on passing from phen or bipy to the NHC ligand.

While investigating the photophysical properties of the *fac*-[Re(CO)$_3$(NHC)L] complexes, we have also serendipitously discovered that photochemical CO dissociation can occur in some instances upon excitation.[17] This type of photochemical transformation had been studied before for tricarbonyl Re(I) complexes bound to ligands possessing a strong *trans* effect such as phosphines, phosphites, and isonitriles.[18−25] More specifically, the CO dissociation has been proposed to occur from a thermally accessible reactive state of triplet ligand field character (^{3}LF), following a dissociative mechanism without rearrangement of the two remaining CO ligands.[21] The bonding properties of NHC ligands are often regarded as analogous to P-based ligands;[26] in this respect, the carbene C atom is capable of promoting the labilization of the ligand in a *trans* position due to its good σ-donation properties. However, our preliminary investigation on the photochemical properties of Re NHC complexes revealed that a dissociative mechanism from a thermally activated ^{3}LF reactive state alone does not adequately describe the loss of CO in a position *trans* to the carbene C atom upon photoexcitation.[17] In fact, three distinct photochemical products are obtained and they have been identified as a tricarbonyl acetonitrile-solvated complex and two different dicarbonyl complexes. Moreover, the CO dissociation is solvent-dependent, as it was found to proceed in acetonitrile but not in coordinating acetone or noncoordinating chloroform. Our studies also revealed that lowering the relative energy of the lowest ^{3}MLCT state, achieved by exchanging the pyridyl-substituted NHC ligand with an analogous quinolyl-substituted NHC ligand, renders the complexes photostable.[17]

To further our studies on the photochemical CO dissociation of *fac*-[Re(CO)$_3$(NHC)L] complexes with the aim of gaining more detailed information on the photochemical mechanism and nature of the reactive excited state, we have prepared a family of complexes (schematized in Figure 1) by varying the substituents bound to the N3 (butyl, phenyl, and mesityl) and N1 (pyridyl, pyrimidyl, and quinoxyl) atoms of the NHC imidazole ring. The ancillary ligand L was also changed between chloro and bromo. Furthermore, we have monitored

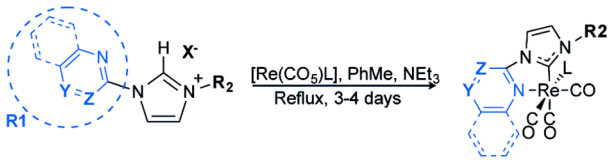

	R1	R2	X	L
1Cl[a]	pyridyl (Y=CH; Z=CH)	n-butyl	Br	Cl
1Br	pyridyl (Y=CH; Z=CH)	n-butyl	Br	Br
2Cl	pyridyl (Y=CH; Z=CH)	mesityl	Cl	Cl
2Br	pyridyl (Y=CH; Z=CH)	mesityl	Br	Br
3Cl	pyrimidyl (Y=CH; Z=N)	mesityl	Cl	Cl
3Br	pyrimidyl (Y=CH; Z=N)	mesityl	PF_6	Br
4Cl	pyrimidyl (Y=CH; Z=N)	phenyl	Cl	Cl
4Br	pyrimidyl (Y=CH; Z=N)	phenyl	PF_6	Br
5Cl	quinoxyl (Y=N; Z=CH)	phenyl	Cl	Cl
5Br	quinoxyl (Y=N; Z=CH)	phenyl	PF_6	Br

Figure 1. General synthetic pathway for the synthesis of the complexes. [a]Complex **1Cl** was prepared using a silver transmetalation protocol.

the photochemical reaction at 293 and 233 K in degassed acetonitrile solutions. The intent of this investigation is to understand how the specific chemical nature of the complex is linked to its photophysical and photochemical properties.

EXPERIMENTAL SECTION

General Procedures. All reagents and solvents were purchased from Sigma Aldrich and Alfa Aesar and used as received without further purification. All of the reactions were performed under a nitrogen atmosphere using standard Schlenk techniques. 1-Mesitylimidazole,[27] 1-phenylimidazole,[28] 1-(2-pyridyl)-3-butylimidazolium bromide,[29] 1-(2-pyridyl)-3-(2,4,6-trimethylphenyl)imidazolium bromide,[30] 1-(2-pyridyl)-3-(2,4,6-trimethylphenyl)imidazolium chloride,[31] and **3Cl**[16] were prepared according to previously published procedures. Deactivated acidic alumina of Brockmann II activity was prepared by adding water to Brockmann I alumina at a ratio of 3% w/w, shaking until clumping stopped, and leaving in a sealed container for 2 days. Nuclear magnetic resonance spectra were recorded using a Bruker Avance 400 spectrometer (400.1 MHz for ^{1}H; 100 MHz for ^{13}C) at 300 K. All of the NMR spectra were calibrated to residual solvent signals. Infrared spectra were recorded using an attenuated total reflectance Perkin-Elmer Spectrum 100 FT-IR with a diamond stage. IR spectra were recorded from 4000 to 650 cm^{-1}. The intensities of the IR bands are reported as strong (s), medium (m), or weak (w), with broad (br) bands also specified. Melting points were determined using a BI Barnsted Electrothermal 9100 apparatus. Elemental analyses were obtained at the Central Science Laboratory, University of Tasmania, using a Thermo Finnigan EA 1112 Series Flash instrument. The imidazolium chloride salts were found to be slightly hygroscopic, and the theoretical elemental analyses had to be adjusted by adding water molecules.

Photophysical Measurements. Absorption spectra were recorded at room temperature using a Perkin-Elmer Lambda 35 UV/vis spectrometer. Uncorrected steady-state emission and excitation spectra were recorded on an Edinburgh FLSP920 spectrometer equipped with a 450 W xenon arc lamp, double-excitation and single-emission monochromators, and a Peltier cooled Hamamatsu R928P photomultiplier tube (185−850 nm). Emission and excitation spectra were corrected for source intensity (lamp and grating) and emission spectral response (detector and grating) by a calibration curve supplied with the instrument. According to the approach described by Demas and Crosby,[32] luminescence quantum yields (Φ) were measured in optically dilute solutions (OD < 0.1 at excitation wavelength) obtained from absorption spectra on a wavelength scale [nm] and compared to the reference emitter by the equation[33]

$$\Phi_x = \Phi_r\left[\frac{A_r(\lambda_r)}{A_x(\lambda_x)}\right]\left[\frac{I_r(\lambda_r)}{I_x(\lambda_x)}\right]\left[\frac{n_x^2}{n_r^2}\right]\left[\frac{D_x}{D_r}\right]$$

where A is the absorbance at the excitation wavelength (λ), I is the intensity of the excitation light at the excitation wavelength (λ), n is the refractive index of the solvent, D is the integrated intensity of the luminescence, and Φ is the quantum yield. The subscripts r and x refer to the reference and the sample, respectively. The quantum yield determinations were performed at identical excitation wavelengths for the sample and the reference, therefore canceling the $I(\lambda_r)/I(\lambda_x)$ term in the equation. All of the complexes were measured against an air-equilibrated aqueous solution of [Ru(bpy)$_3$]Cl$_2$ used as reference (Φ_r = 0.028), with the exception of **1Cl** and **2Cl**, which were measured against an air-equilibrated ethanol solution of rhodamine 101 (Φ_r = 1.0).[33,34] Emission lifetimes (τ) were determined with the single photon counting technique (TCSPC) with the same Edinburgh FLSP920 spectrometer using a pulsed picosecond diode laser "(EPL 375, fwhm < 800 ps) as the excitation source, with repetition rates between 10 kHz and 1 MHz, and the aforementioned R928P PMT as detector. The goodness of fit was assessed by minimizing the reduced χ^2 function and by visual inspection of the weighted residuals. To record the 77 K luminescence spectra, the samples were put in glass tubes (2 mm diameter) and inserted in a special quartz Dewar filled

dx.doi.org/10.1021/ic403138a | Inorg. Chem. 2014, 53, 3629−3641

with liquid nitrogen. The dichloromethane solvent used in the preparation of the solutions for the photophysical investigations was of spectrometric grade. All of the prepared solutions were filtered through a 0.2 μm syringe filter before measurement. Degassed samples were prepared by the freeze−pump−thaw technique. Temperature-dependent lifetime measurements were obtained with an Edinburgh FLS980-stm spectrometer equipped with a temperature-controlled cuvette holder, for measurements between 293 and 333 K, or a liquid nitrogen cooled Oxford Instrument OptiscanDN cryostat, for measurements below room temperature. Experimental uncertainties are estimated to be ±8% for lifetime determinations, ±20% for quantum yields, and ±2 and ±5 nm for absorption and emission peaks, respectively.

Photolysis Experiments. The complexes (~5 mg) were dissolved in CD_3CN (1.5 mL), and an initial ^{1}H NMR spectrum was acquired. The solution was then transferred to a quartz cuvette, and 99 consecutive emission spectra with an excitation wavelength of 370 nm were collected on a Hitachi F-4600 luminescence spectrophotometer for approximately 4 h. The following parameters were set: sweep width 200−800 nm, excitation slit width 20 nm, and emission slit width 5 nm. A second ^{1}H NMR spectrum was acquired of the photolyzed solutions. An IR spectrum was then collected by slow addition of small droplets of the solution onto the diamond stage of the Perkin-Elmer Spectrum 100 FT-IR spectrometer. The solution was allowed to evaporate, and the dropping procedure was repeated until a sample concentrated enough to allow collection of an IR spectrum was obtained. The IR spectrum of the photolyzed sample was overlaid with the IR spectrum of the same rhenium compound in DMSO, as the poor solubility of the starting material in acetonitrile produced poor-quality spectra. Temperature-dependent photolysis studies were obtained in a similar procedure on an Edinburgh FLSP980-stm spectrometer equipped with a temperature-controlled cuvette holder, for experiments between 293 and 333 K, or liquid nitrogen cooled Oxford Instrument OptiscanDN cryostat, for experiments below room temperature.

Synthesis of 1-(2-Pyrimidyl)-3-(2,4,6-trimethylphenyl)-imidazolium Chloride. The same procedure used for the preparation of 1-(2-pyridyl)-3-(2,4,6-trimethylphenyl)imidazolium chloride was followed with the following modifications: 2-chloropyrimidine was substituted for 2-chloropyridine, and the reaction temperature was set to 140 °C to afford a light brown solid (61%). Mp: 272−275 °C. Anal. Calcd for $C_{16}H_{17}ClN_4 \cdot 1.15H_2O$: C, 59.77; H, 6.05; N, 17.44. Found C, 59.34; H, 5.85; N, 17.88. ^{1}H NMR (DMSO-d_6): δ 10.48 (1H, app t, splitting 1.6 Hz, NC*H*N), 9.10 (2H, d, J = 5.2 Hz, pyrimidyl *H4*, *H6*), 8.77 (1H, app t, splitting 2.0 Hz, imidazoyl C*H*), 8.19 (1H, app t, splitting 2.0 Hz, imidazoyl C*H*), 7.82 (1H, t, J = 4.8 Hz, pyrimidyl *H5*), 7.18 (2H, s, phenyl *meta-H*), 2.35 (3H, s, CH_3), 2.11 (6H, s, CH_3) ppm. ^{13}C NMR (DMSO-d_6): δ 160.0 (2 × pyrimidyl *C*H; *C4, C6*), 152.3 (pyrimidyl quat *C*1), 140.4 (phenyl quat *C*1), 137.2 (NCHN), 134.3 (phenyl quat *C*2, *C*6), 131.2 (phenyl quat *C*4), 129.2 (2 × phenyl CH), 125.3 (imidazoyl CH), 122.6 (pyrimidyl CH; *C5*), 120.1 (imidazoyl CH), 20.6 (CH_3), 17.0 (CH_3), 16.9 (CH_3) ppm. ATR-IR: ν 3421 w, 3363 w, 3255 w, 3189 w, 3160 m, 3122 m, 3049 m, 2978 m, 2918 s, 2753 w, 2324 w, 2287 w, 2193 w, 2162 w, 2152 w, 2103 w, 2067 w, 2050 w, 1823 w, 1628 w, 1605 w, 1584 s, 1561 w, 1521 s, 1489 w, 1450 w, 1412 s, 1377 m, 1344 w, 1327 w, 1307 w, 1291 w, 1248 w, 1191 w, 1120 w, 1101 w, 1073 w, 1051 w, 998 w, 971 w, 934 w, 902 w, 884 w, 852 w, 841 w, 790 w, 767 w, 738 w, 674 w cm^{-1}.

Synthesis of 1-(2-Pyrimidyl)-3-(2,4,6-trimethylphenyl)-imidazolium Hexafluorophosphate. A saturated aqueous solution of potassium hexafluorophosphate was added to an aqueous solution of 1-(2-pyrimidyl)-3-(2,4,6-trimethylphenyl)imidazolium chloride until precipitation ceased. The resulting solid was used in the following reaction without further purification or characterization.

Synthesis of 1-(2-Pyrimidyl)-3-phenylimidazolium Chloride. The same procedure used for the preparation of 1-(2-pyridyl)-3-(2,4,6-trimethylphenyl)imidazolium chloride was followed with the following modifications: 2-chloropyrimidine was substituted for 2-chloropyridine, 1-phenylimidazole was substituted for 1-(2,4,6-trimethylphenyl)-imidazole, and the reaction temperature was set to 140 °C to afford a light brown solid (87%). Mp: 224−227 °C. Anal. Calcd for $C_{13}H_{11}ClN_4 \cdot H_2O$: C, 56.42; H, 4.74; N, 20.25. Found C, 56.29; H, 4.58; N, 20.56. ^{1}H NMR (DMSO-d_6): δ 10.70 (1H, app t, splitting 2.0 Hz, NC*H*N), 9.12 (2H, d, J = 4.8 Hz, pyrimidyl *H4*, *H6*), 8.75 (1H, app t, splitting 2.0 Hz, imidazoyl C*H*), 8.57 (1H, app t, splitting 2.0 Hz, imidazoyl C*H*), 7.99−7.96 (2H, m, phenyl *ortho-H*), 7.84 (1H, t, J = 4.8 Hz, pyrimidyl *H5*), 7.72−7.65 (3H, m, phenyl *meta-H*, *para-H*) ppm. ^{13}C NMR (DMSO-d_6): δ 160.2 (2 × pyrimidyl *C*H; *C4, C6*), 152.2 (pyrimidyl quat *C1*), 135.0 (NCHN), 134.5 (phenyl quat *C*), 130.4 (phenyl CH), 130.1 (2 × phenyl CH), 122.9 (imidazoyl CH), 122.8 (pyrimidyl CH; *C5*), 122.6 (2 × phenyl CH), 120.0 (imidazoyl CH) ppm. ATR-IR: ν 3140 m, 3015 m, 2324 w, 2163 w, 2105 w, 1660 w, 1587 m, 1561 w, 1536 s, 1496 w, 1467 w, 1418 s, 1387 m, 1351 w, 1337 w, 1311 w, 1275 w, 1242 m, 1190 w, 1165 w, 1144 w, 1119 w, 1057 w, 1001 w, 977 w, 951 w, 914 w, 816 w, 788 w, 763 m, 737 w, 684 w cm^{-1}.

Synthesis of 1-(2-Pyrimidyl)-3-phenylimidazolium Hexafluorophosphate. A saturated aqueous solution of potassium hexafluorophosphate was added to an aqueous solution of 1-(2-pyrimidyl)-3-phenylimidazolium chloride until precipitation ceased. The resulting solid was used in the following reaction without further purification or characterization.

Synthesis of 1-(2-Quinoxyl)-3-phenylimidazolium Chloride. The same procedure used for the preparation of 1-(2-pyridyl)-3-(2,4,6-trimethylphenyl)imidazolium chloride was followed with the following modifications: 2-chloroquinoxaline was substituted for 2-chloropyridine, 1-phenylimidazole was substituted for 1-(2,4,6-trimethylphenyl)-imidazole, and the reaction temperature was set to 140 °C to afford a black powder (78%). Mp: 287−289 °C. Anal. Calcd for $C_{17}H_{13}N_4Cl \cdot 0.3H_2O$: C, 64.99; H, 4.36; N, 17.83. Found: C, 64.90; H, 4.03; N, 17.70. ^{1}H NMR (DMSO-d_6): δ 11.20 (1H, app t, splitting 1.6 Hz, NC*H*N), 9.93 (1H, s, quinoxyl C*H*), 8.96 (1H, app t, splitting 1.8 Hz, imidazoyl C*H*), 8.74 (1H, app t, splitting 1.8 Hz, imidazoyl C*H*), 8.30−8.19 (1H, m, quinoxyl C*H*), 8.22−8.19 (1H, m, quinoxyl C*H*), 8.09−8.01 (4H, m, 2 × phenyl C*H*, 2 × quinoxyl C*H*), 7.77−7.65 (3H, m, 3 × phenyl C*H*) ppm. ^{13}C NMR (DMSO-d_6): δ 120.2 (imidazoyl CH), 121.9 (phenyl CH), 122.3 (imidazoyl CH), 128.6 (quinoxyl CH), 129.2 (quinoxyl CH), 130.0 (phenyl CH), 130.2 (phenyl CH), 130.4 (quat phenyl C), 131.6 (quinoxyl CH), 132.4 (quinoxyl CH), 134.5 (quat quinoxyl C), 135.5 (imidazoyl NCHN), 138.9 (quinoxyl C), 141.2 (quat quinoxyl C), 141.8 (quat quinoxyl C) ppm. ATR-IR: ν 3150 w, 3066 w, 3016 w, 2949 w, 2814 w, 1657 w, 1598 w, 1584 w, 1548 m, 1499 m, 1433 w, 1400 w, 1373 w, 1349 w, 1318 m, 1289 m, 1274 m, 1234 m, 1206 w, 1149 w, 1133 w, 1116 w, 1104 w, 1062 w, 1013 w, 1001 w, 959 w, 942 w, 895 w, 853 w, 771 w, 752 m, 677 m cm^{-1}.

Synthesis of 1-(2-Quinoxyl)-3-phenylimidazolium Hexafluorophosphate. A saturated aqueous solution of potassium hexafluorophosphate was added to an aqueous solution of 1-(2-quinoxyl)-3-phenylimidazolium chloride until precipitation ceased. The resulting solid was used in the following reaction without further purification or characterization.

Synthesis of 1Cl. A suspension of 1-butyl-3-(2-pyridyl)-imidazolium bromide (408 mg, 1.45 mmol) and Ag_2O (375 mg, 1.62 mmol) in dichloromethane (20 mL) was stirred in darkness at room temperature for 48 h, after which $[Re(CO)_5Cl]$ (346 mg, 0.95 mmol) was added and the reaction mixture was heated at reflux under an inert atmosphere for 4 days. The resulting green solution was filtered through a short plug of deactivated acidic alumina and washed with dichloromethane (50 mL) followed by acetonitrile (50 mL). The combined fractions were concentrated in vacuo and washed with diethyl ether (50 mL) to afford a yellow solid (178 mg, 37%). Crystals suitable for a single-crystal X-ray diffraction study were grown by slow diffusion of diethyl ether into a solution of the compound in chloroform. Mp: 198 °C dec. Anal. Calcd for $C_{15}ClH_{15}N_3O_3Re$: C, 35.54; H, 2.98; N, 8.29. Found: C, 35.19; H, 2.50; N, 7.90. ^{1}H NMR (DMSO-d_6): δ 8.83 (1H, d, J = 5.2 Hz, pyridyl *H6*), 8.45 (1H, d, J = 2.0 Hz, imidazoyl C*H*), 8.35−8.25 (2H, m, 2 × pyridyl C*H*), 7.74 (1H, d, J = 2.4 Hz, imidazoyl C*H*), 7.53−7.49 (1H, m, pyridyl C*H*), 4.23

dx.doi.org/10.1021/ic403138a | *Inorg. Chem.* 2014, 53, 3629−3641

(2H, t, J = 7.2 Hz, NCH_2), 1.88−1.83 (2H, m, $CH_3CH_2CH_2$), 1.40−1.35 (2H, m, CH_3CH_2), 0.93 (3H, t, J = 7.6 Hz, CH_3) ppm. ^{13}C NMR (DMSO-d_6): δ 198.9 (CO), 198.0 (CO) 190.0 (NCN), 189.2 (CO), 153.2 (pyridyl CH), 152.6 (pyridyl quat C), 142.3 (pyridyl CH), 124.0 (pyridyl CH), 124.0 (imidazoyl CH), 117.5 (imidazoyl CH), 112.8 (pyridyl CH), 51.0 (NCH_2), 32.7 ($CH_2CH_2CH_3$), 19.1 (CH_2CH_3), 13.6 (CH_3) ppm. ATR-IR: ν 3937 w, 3775 w, 3164 w, 3114 w, 3092 w, 3060 w, 3030 w, 2964 w, 2935 w, 2864 w, 2017 s (CO), 1918 s (CO), 1871 s (CO), 1710 w, 1615 w, 1575 w, 1558 w, 1487 m, 1464 w, 1450 w, 1429 w, 1384 w, 1370 w, 1331 w, 1288 w, 1263 w, 1249 w, 1197 w, 1159 w, 1146 w, 1128 w, 1107 w, 1091 w, 1033 w, 1022 w, 1001 w, 910 w, 886 w, 856 w, 778 w, 754 w, 702 w, 691 w cm^{-1}.

Synthesis of 1Br. A suspension of [Re(CO)$_5$Br] (445 mg, 1.09 mmol), 1-butyl-3-(2-pyridyl)imidazolium bromide (305 mg, 1.08 mmol), and triethylamine (1.5 mL, 10.8 mmol) in toluene (ca. 10 mL) was heated at reflux for 2 days. The resulting mixture was cooled to room temperature, water (ca. 5 mL) and hexanes (ca. 7 mL) were added, and eventually the hexanes layer was removed. The aqueous layer was then extracted with dichloromethane, and the organic phase was collected, dried over $MgSO_4$, and evaporated to dryness. The crude product was then purified by flash column chromatography on deactivated acidic alumina with dichloromethane as the eluting solvent (327 mg, 55%). Mp: 192 °C dec. Anal. Calcd for $C_{15}H_{15}N_3O_3ReBr$: C, 32.67; H, 2.74; N, 7.62. Found: C, 32.69; H, 2.71; N, 7.65. ^{1}H NMR ($CDCl_3$): δ 8.90 (1H, d, J = 5.6 Hz, pyridyl *H6*), 8.00 (1H, dd, J = 1.6 Hz, J = 8.0 Hz, pyridyl C*H*), 7.57−7.56 (2H, m, imidazoyl C*H* and pyridyl C*H*), 7.29 (1H, dd, J = 1.6 Hz, J = 6.8 Hz, pyridyl C*H*), 7.08 (1H, d, J = 2.4 Hz, imidazoyl C*H*), 4.35−4.23 (2H, m, NCH_2), 2.04−1.92 (2H, m, $CH_2CH_2CH_2$), 1.51−1.46 (2H, m, CH_3CH_2) 1.01 (3H, t, J = 7.6 Hz, CH_3) ppm. ^{13}C NMR ($CDCl_3$): δ 197.3 (CO), 196.8 (CO), 193.0 (NCN), 188.0 (CO), 153.9 (pyridyl CH), 152.9 (pyridyl quat C), 140.7 (pyridyl CH), 123.2 (pyridyl CH), 123.1 (imidazoyl CH), 115.8 (imidazoyl CH), 111.5 (pyridyl CH), 52.4 (NCH_2), 33.0 ($CH_2CH_2CH_3$), 19.8 (CH_2CH_3), 13.7 (CH_3) ppm. ATR-IR: ν 3905 w, 3748 w, 3164 w, 3118 w, 3095 w, 3067 w, 3039 w, 2964 w, 2942 w, 2867 w, 2014 s (CO), 1915 s (CO), 1887 s (CO), 1681 w, 1615 m, 1578 w, 1489 m, 1456 m, 1430 m, 1386 w, 1375 w, 1364 w, 1331 m, 1314 w, 1299 w, 1257 w, 1197 w, 1166 w, 1144 w, 1130 w, 1103 w, 1091 w, 1022 w, 1006 w, 958 w, 908 w, 892 w, 780 w, 747 w, 732 w, 704 w, 690 w cm^{-1}.

Synthesis of 2Cl. The target complex was prepared following the same procedure reported for **1Br**, but starting from [Re(CO)$_5$Cl], using 1-(2-pyridyl)-3-(2,4,6-trimethylphenyl)imidazolium chloride as the starting imidazolium salt (32 mg, 49%). Crystals suitable for a single-crystal X-ray diffraction study were grown from slow evaporation of an acetonitrile solution of **2Cl**. Mp: 235 °C dec. Anal. Calcd for $C_{20}H_{17}N_3O_3ReCl$: C, 42.21; H, 3.01; N, 7.39. Found: C, 42.03; H, 2.89; N, 7.21. ^{1}H NMR ($CDCl_3$): δ 8.92 (1H, d, J = 7.8 Hz, pyridyl C*H*), 8.07 (1H, dd, J = 1.6 Hz, J = 8.0 Hz, pyridyl C*H*), 7.75 (1H, d, J = 2.4 Hz, imidazoyl C*H*), 7.64 (1H, d, J = 8.4 Hz, pyridyl C*H*), 7.64 (1H, d, J = 8.4 Hz, pyridyl C*H*), 7.34 (1H, dd, J = 1.2 Hz, J = 6.6 Hz, pyridyl C*H*), 7.07−7.06 (3H, m, imidazoyl C*H*, mesityl C*H*), 2.38 (3H, s, 4-mesityl CH_3), 2.25 (3H, s, 2,6-mesityl CH_3), 2.14 (3H, s, 2,6-mesityl CH_3) ppm. ^{13}C NMR ($CDCl_3$): δ 197.7 (CO), 196.8 (CO), 194.7 (NCN), 188.7 (CO), 154.2 (pyridyl CH), 153.3 (pyridyl quat C), 140.8 (pyridyl CH), 140.3 (4-mesityl quat C), 136.3 (2,6-mesityl quat C), 135.2 (1-mesityl quat C), 134.8 (2,6-mesityl quat C), 129.8 (3,5-mesityl CH), 129.3 (3,5-mesityl CH), 124.3 (imidazoyl CH), 123.6 (pyridyl CH), 116.3 (imidazoyl CH), 111.7 (pyridyl CH), 21.3 (4-mesityl CH_3), 18.5 (2,6-mesityl CH_3), 17.8 (2,6-mesityl CH_3) ppm. ATR-IR: ν 3089 w, 2924 w, 2010 s (CO), 1909 s (CO), 1867 s (CO), 1615 m, 1544 w, 1515 w, 1483 m, 1453 w, 1421 m, 1379 w, 1343 w, 1315 w, 1265 w, 1237 w, 1160 w, 1135 w, 1036 w, 910 w, 850 w, 771 w, 703 w cm^{-1}.

Synthesis of 2Br. The target complex was prepared following the same procedure as for **1Br**, using 1-(2-pyridyl)-3-(2,4,6-trimethylphenyl)imidazolium bromide as the starting imidazolium salt (199 mg, 66%). Crystals suitable for a single-crystal X-ray diffraction study were grown from slow evaporation of an acetonitrile solution of **2Br**. Mp: 243 °C dec. Anal. Calcd for $C_{20}H_{17}N_3O_3ReBr$: C, 39.16; H, 2.79; N, 6.85. Found: C, 39.22; H, 2.62; N, 6.79. ^{1}H NMR ($CDCl_3$): δ 8.92 (1H, d, J = 6.0 Hz, pyridyl C*H*), 8.08−8.03 (1H, m, pyridyl C*H*), 7.77 (1H, d, J = 2.4 Hz, imidazoyl C*H*), 7.64 (1H, d, J = 8.0 Hz, pyridyl C*H*), 7.33−7.31 (1H, m, pyridyl C*H*), 7.07−7.06 (3H, m, imidazoyl C*H*, mesityl C*H*), 2.37 (3H, s, 4-mesityl CH_3), 2.29 (3H, s, 2,6-mesityl CH_3), 2.13 (3H, s, 2,6-mesityl CH_3) ppm. ^{13}C NMR ($CDCl_3$): δ 196.9 (CO), 195.9 (CO), 194.2 (NCN), 188.2 (CO), 154.3 (pyridyl CH), 153.2 (pyridyl quat C), 140.7 (pyridyl CH), 140.3 (4-mesityl C), 136.2 (2,6-mesityl C), 134.8 (2,6-mesityl C), 129.8 (2,5-mesityl CH), 129.3 (2,5-mesityl CH), 124.4 (imidazoyl CH), 123.5 (pyridyl CH), 116.3 (imidazoyl CH), 111.7 (pyridyl CH), 21.3 (4-mesityl CH_3), 19.0 (2,6-mesityl CH_3), 17.8 (2,6-mesityl CH_3) ppm. ATR-IR: ν 3919 w, 3169 w, 3148 w, 3117 w, 3091 w, 3039 w, 2977 w, 2923 w, 2856 w, 2407 w, 2011 s (CO), 1918 s (CO), 1870 s (CO), 1616 m, 1575 w, 1558 w, 1484 m, 1453 w, 1439 w, 1419 w, 1378 w, 1342 w, 1314 w, 1266 w, 1159 w, 1135 w, 1111 w, 1093 w, 1083 w, 1038 w, 977 w, 953 w, 934 w, 872 w, 848 w, 768 w, 747 w, 720 w, 700 w cm^{-1}.

Synthesis of 3Br. The target complex was prepared by following the same procedure as for **1Br**, using 1-(2-pyrimidyl)-3-(2,4,6-trimethylphenyl)imidazolium hexafluorophosphate as the starting imidazolium salt (46 mg, 58%). Mp: 277 °C dec. Anal. Calcd for $C_{19}H_{16}BrN_4O_3Re$: C, 37.14; H, 2.62; N, 9.12. Found: C, 37.45; H, 2.66; N, 8.94. ^{1}H NMR (DMSO-d_6): δ 9.24−9.22 (1H, m, pyrimidyl *H6*), 9.15−9.13 (1H, m, pyrimidyl *H4*), 8.45 (1H, d, J = 2.0 Hz, imidazoyl C*H*), 7.76 (1H, d, J = 2.4 Hz, imidazoyl C*H*), 7.64 (1H, t, J = 5.2 Hz, pyrimidyl *H5*), 7.13 (1H, s, mesityl C*H*), 7.10 (1H, s, mesityl C*H*), 2.33 (1H, s, CH_3), 2.17 (1H, s, CH_3), 2.07 (1H, s, CH_3) ppm. ^{13}C NMR (100 MHz, DMSO-d_6): δ 196.7 (CO), 194.9 (CO), 191.2 (NCN), 188.1 (CO), 163.1 (pyrimidyl CH), 161.0 (pyrimidyl CH), 157.7 (pyrimidyl quat C), 139.2 (phenyl quat C), 135.3 (phenyl quat C), 134.8 (phenyl quat C), 134.4 (phenyl quat C), 129.0 (phenyl CH), 128.8 (phenyl CH), 125.4 (imidazoyl CH), 120.8 (pyrimidyl CH; *C5*), 118.6 (imidazoyl CH), 20.7 (CH_3), 18.1 (CH_3), 17.1 (CH_3) ppm. ATR-IR: ν 3926 w, 3685 w, 3676 w, 3182 w, 2988 m, 2973 m, 2912 m, 2902 m, 2747 w, 2410 w, 2324 w, 2489 w, 2012 s (CO), 1921 s (CO), 1883 s (CO), 1595 m, 1568 w, 1557 w, 1512, 1470 m, 1449 m, 1411 w, 1394 w, 1379 w, 1343 w, 1306 w, 1257 w, 1197 w, 1168 w, 1139 w, 1058 w, 1028 w, 978 w, 963 w, 934 w, 848 w, 809 w, 788 w, 744 w, 699 w, 655 w cm^{-1}.

Synthesis of 4Cl. The target complex was prepared following the same procedure as for **1Br**, but starting from [Re(CO)$_5$Cl], with 1-(2-pyrimidyl)-3-(phenyl)imidazolium chloride as the starting imidazolium salt (43 mg, 58%). Crystals suitable for a single-crystal X-ray diffraction study were grown from slow evaporation of an acetonitrile solution of **4Cl**. Mp: 249 °C dec. Anal. Calcd for $C_{16}H_{10}ClN_4O_3Re$: C, 36.40; H, 1.91; N, 10.61. Found: C, 36.10; H, 1.94; N, 10.42. ^{1}H NMR (DMSO-d_6): δ 9.27−9.25 (1H, m, pyrimidyl *H6*), 9.17−9.16 (1H, m, pyrimidyl *H4*), 8.42 (1H, d, J = 2.0 Hz, imidazoyl C*H*), 8.01 (1H, d, J = 2.0 Hz, imidazoyl C*H*), 7.71−7.61 (6H, m, pyrimidyl *H5*, phenyl *ortho-H*, *meta-H*, *para-H*) ppm. ^{13}C NMR (DMSO-d_6): δ 197.3 (CO), 196.5 (CO), 190.4 (NCN), 188.6 (CO), 162.8 (pyrimidyl CH), 161.2 (pyrimidyl CH), 157.7 (pyrimidyl quat C), 138.6 (phenyl quat C), 129.7 (phenyl CH), 129.6 (2 × phenyl CH), 126.0 (2 × phenyl CH), 125.4 (imidazoyl CH), 121.0 (pyrimidyl CH), 118.3 (imidazoyl CH) ppm. ATR-IR: ν 3175 w, 3145 w, 3067 w, 2020 s (CO), 1913 s (CO), 1865 s (CO), 1596 m, 1568 m, 1500 w, 1470 m, 1446 m, 1416 m, 1378 m, 1346 m, 1320 m, 1301 w, 1263 m, 1199 w, 1144 w, 1097 w, 1070 w, 1022 w, 979 w, 951 w, 817 w, 787 w, 761 w, 746 m, 690 m, 633 w, 618 w, 527 w cm^{-1}.

Synthesis of 4Br. The target complex was prepared following the same procedure as for **1Br** using 1-(2-pyrimidyl)-3-phenylimidazolium hexafluorophosphate as the starting imidazolium salt (28 mg, 35%). Crystals suitable for a single-crystal X-ray diffraction study were grown from slow evaporation of an acetonitrile solution of **4Br**. Mp: 200 °C dec. Anal. Calcd for $C_{16}H_{10}BrN_4O_3Re{\cdot}0.5CH_2Cl_2$: C, 32.23; H, 1.80; N, 9.11. Found: C, 32.63; H, 1.80; N, 8.77 (despite several attempts, the complex was always isolated as a solvated species; the presence of dichloromethane was also confirmed via ^{1}H NMR). ^{1}H NMR (DMSO-d_6): δ 9.27−9.25 (1H, m, pyrimidyl *H6*), 9.16−9.14 (1H,

dx.doi.org/10.1021/ic403138a | Inorg. Chem. 2014, 53, 3629−3641

m, pyrimidyl *H4*), 8.43 (1H, d, *J* = 2.4 Hz, imidazoyl C*H*), 8.00 (1H, d, *J* = 2.0 Hz, imidazoyl C*H*), 7.72−7.59 (6H, m, pyrimidyl *H5*, phenyl *ortho-H*, *meta-H*, *para-H*) ppm. ^{13}C NMR (DMSO-d_6): δ 196.6 (*C*O), 195.9 (*C*O), 189.4 (*C*N), 188.1 (*C*O), 163.0 (pyrimidyl *C*H), 161.2 (pyrimidyl *C*H), 157.7 (pyrimidyl quat *C*), 138.6 (phenyl quat *C*), 129.7 (phenyl *C*H), 129.6 (2 × phenyl *C*H), 126.1 (2 × phenyl *C*H), 125.5 (imidazoyl *C*H), 120.9 (pyrimidyl *C*H), 118.4 (imidazoyl *C*H) ppm. ATR-IR: ν 3146 w, 2014 s (CO), 1913 s (CO), 1860 s (CO), 1594 m, 1566 m, 1498 w, 1469 m, 1423 m, 1381 m, 1345 m, 1303 w, 1263 w, 1142 w, 1074 w, 978 w, 952 w, 816 w, 788 w, 768 w, 744, 691 w, 634 w cm^{-1}.

Synthesis of 5Cl. The target complex was prepared following the same procedure as for **1Br**, but starting from [Re(CO)$_5$Cl], with 1-(2-quinoxyl)-3-(phenyl)imidazolium chloride as the starting imidazolium salt (176 mg 65%). Mp: 247 °C dec. Anal. Calcd for $C_{20}H_{12}ClN_4O_3Re$: C, 41.56; H, 2.09; N, 9.69. Found: C, 41.72; H, 1.91; N, 9.49. ^{1}H NMR (DMSO-d_6): δ 9.99 (1H, s, quinoxyl C*H*), 9.01 (1H, d, *J* = 2.4 Hz, imidazoyl C*H*), 8.55 (1H, d, *J* = 8.0 Hz, quinoxyl C*H*), 8.35 (1H, dd, *J* = 1.2 Hz, *J* = 8.2 Hz, quinoxyl C*H*), 8.20 (1H, app t, splitting 7.2 Hz, quinoxyl C*H*), 8.13 (1H, d, *J* = 2.4 Hz, imidazoyl C*H*), 8.05 (1H, app t, splitting 7.6 Hz, quinoxyl C*H*), 7.73−7.64 (5H, m, phenyl C*H*) ppm. ^{13}C NMR (DMSO-d_6): δ 197.9 (*C*O) 194.9 (*C*O), 194.0 (*C*N), 188.1 (*C*O), 148.6 (quat quinoxyl *C*), 141.0 (quat quinoxyl *C*), 138.9 (quat quinoxyl *C*), 138.4 (quinoxyl *C*H), 133.3 (quinoxyl *C*H), 130.8 (quinoxyl *C*H), 130.3 (quinoxyl *C*H), 129.8 (phenyl *C*H), 128.1 (quinoxyl *C*H), 126.2 (phenyl *C*H), 125.7 (imidazoyl *C*H), 119.1 (imidazoyl *C*H) ppm. ATR-IR: ν 3164 w, 3114 w, 3024 w, 2013 (CO) s, 1915 (CO) s, 1902 (CO) s, 1851 m, 1675 w, 1597 w, 1569 w, 1544 w, 1497 m, 1478 w, 1442 m, 1428 m, 1392 w, 1359 m, 1327 w, 1293 m, 1261 w, 1234 w, 1219 w, 1173 w, 1157 w, 1137 w, 1115 w, 1101 w, 1023 w, 994 w, 964 w, 944 w, 931 w, 874 w, 855 w, 840 w, 774 w, 759 w, 734 w, 701 w, 688 w, 677 w cm^{-1}.

Synthesis of 5Br. The target complex was prepared following the same procedure as for **1Br** using 1-(2-quinoxyl)-3-(phenyl)-imidazolium hexafluorophosphate as the starting imidazolium salt (30 mg, 46%). Crystals suitable for a single-crystal X-ray diffraction study were grown from slow evaporation of an acetonitrile solution of **5Br**. Mp: 250 °C dec. Anal. Calcd for: $C_{20}H_{12}BrN_4O_3Re$: C, 38.59; H, 1.94; N, 9.00. Found C, 38.44; H, 1.73; N, 8.71. ^{1}H NMR ($CDCl_3$): δ 9.31 (1H, s, quinoxyl C*H*) 8.76 (1H, d, *J* = 8.8 Hz, quinoxyl C*H*), 8.28 (1H, d, *J* = 8.4 Hz, quinoxyl C*H*), 8.08−8.03 (2H, m, quinoxyl C*H*, imidazoyl C*H*), 7.94 (1H, app t, splitting 7.6 Hz, quinoxyl C*H*), 7.73−7.62 (5H, m, phenyl C*H*), 7.41 (1H, d, *J* = 2.0 Hz, imidazoyl C*H*) ppm. ^{13}C NMR ($CDCl_3$): δ 197.2 (*C*O), 196.4 (*C*O), 193.2 (*C*N), 186.8 (*C*O), 147.7 (quat quinoxyl *C*), 142.1 (quat quinoxyl *C*), 140.3 (quat quinoxyl *C*), 139.1 (quat phenyl *C*), 134.7 (quinoxyl *C*H), 134.0 (quinoxyl *C*H), 131.2 (quinoxyl *C*H), 130.7 (quinoxyl *C*H), 130.5 (phenyl *C*H), 130.2 (2 × phenyl *C*H), 129.7 (quinoxyl *C*H), 126.8 (2 × phenyl *C*H), 125.6 (imidazoyl *C*H), 116.5 (imidazoyl *C*H) ppm. ATR-IR: ν 3083 w, 2023 s (CO), 1938 s (CO), 1894 s (CO), 1596 w, 1542 w, 1495 m, 1475 w, 1438 m, 1421 w, 1359 w, 1333 w, 1300 w, 1231 w, 1212 w, 1154 w, 1119 w, 1023 w, 996 w, 964 w, 944 w, 919 w, 893 w, 856 w, 764 w, 690 w cm^{-1}.

X-ray Crystallography. Crystallographic data for the structures were collected at 100(2) K (150(2) K for **1Cl**) on an Oxford Diffraction Gemini diffractometer fitted with either Mo Kα radiation (for **1Cl** and **2Br**) or Cu Kα radiation (for **5Br**) and a Oxford Diffraction Xcalibur diffractometer fitted with Mo Kα radiation (for **2Cl**, **4Cl**, and **4Br**). Following analytical absorption corrections and solution by direct methods, the structures were refined against F^2 with full-matrix least squares using the program SHELXL-97.[35] Unless stated below, anisotropic displacement parameters were employed for the non-hydrogen atoms. All hydrogen atoms were added at calculated positions and refined by use of a riding model with isotropic displacement parameters based on those of the parent atom. Selected collection and refinement data are given below together with CCDC numbers. Supplementary crystallographic data can be obtained free of charge via http://www.ccdc.cam.ac.uk/conts/retrieving.html or from the Cambridge Crystallographic Data Centre, 12 Union Road, Cambridge CB2 1EZ, U.K.: fax, (+44) 1223-336-033; e-mail, deposit@ccdc.cam.ac.uk.

X-ray data refinement for ***1Cl****:* empirical formula $C_{15}H_{15}ClN_3O_3Re$, formula weight 506.95, λ = 0.71073 Å, monoclinic, space group $P2_1/c$, *a* = 18.0965(4) Å, *b* = 10.2473(2) Å, *c* = 9.2381(2) Å, β = 90.810(2)°, *V* = 1712.94(6) Å^3, *Z* = 4, D_{calcd} = 1.966 Mg/m^3, μ = 7.266 mm^{-1}, crystal size 0.26 × 0.17 × 0.05 mm^3, $2\theta_{max}$ = 76.00°, 66202 reflections collected, 9297 independent reflections (R_{int} = 0.0471), T_{max}/T_{min} = 0.704/0.362, 9297/24/228 data/restraints/parameters, goodness of fit on F^2 1.092, final *R* indices ($I > 2\sigma(I)$) R1 = 0.0309 and wR2 = 0.0569, *R* indices (all data) R1 = 0.0453 and wR2 = 0.0603, largest difference peak and hole 2.619 and −1.293 e/Å^3, CCDC 974868. The two terminal atoms of the butyl chain are disordered over two sets of sites with occupancies constrained to 0.5 after trial refinement.

X-ray data refinement for ***2Cl****:* empirical formula $C_{20}H_{17}ClN_3O_3Re$, formula weight 569.02, λ = 0.71073 Å. monoclinic, space group $P2_1/n$, *a* = 8.1644(7) Å, *b* = 17.6255(17) Å, *c* = 13.6343(15) Å, β = 97.645(9)°, *V* = 1944.6(3) Å^3. *Z* = 4, D_{calcd} = 1.944 Mg/m^3, μ = 6.413 mm^{-1}, crystal size 0.12 × 0.08 × 0.07 mm^3, $2\theta_{max}$ = 56°, 17569 reflections collected, 4689 independent reflections (R_{int} = 0.0629), T_{max}/T_{min} = 0.694/0.604, 4689/18/272 data/restraints/parameters, final *R* indices ($I > 2\sigma(I)$) R1 = 0.0620 and wR2 = 0.1266, *R* indices (all data) R1 = 0.0758 and wR2 = 0.1326, largest difference peak and hole 4.276 and −1.824 e/Å^3, CCDC 974869. The Cl atom is positionally disordered with the carbonyl group in the *trans* position with site occupancies refined to 0.687(14) and its complement. The geometries of the disordered carbonyl groups were restrained to ideal values.

X-ray data refinement for ***2Br****:* empirical formula $C_{20}H_{17}BrN_3O_3Re$, formula weight 613.48, λ = 0.71073 Å, monoclinic, space group $P2_1/n$, *a* = 8.2661(2) Å, *b* = 17.5306(3) Å, *c* = 13.6552(4) Å, β = 97.690(2)°, *V* = 1960.97(8) Å^3, *Z* = 4, D_{calcd} = 2.078 Mg/m^3, μ = 8.261 mm^{-1}, crystal size 0.29 × 0.21 × 0.15 mm^3, $2\theta_{max}$ = 73°, 48086 reflections collected, 9217 independent reflections (R_{int} = 0.0405), T_{max}/T_{min} = 0.341/0.166, 9217/6/272 data/restraints/parameters, final *R* indices ($I > 2\sigma(I)$) R1 = 0.0484 and wR2 = 0.0764, *R* indices (all data) R1 = 0.0761 and wR2 = 0.0807, largest difference peak and hole 3.912 and −6.113 e/Å^3, CCDC 974870. The Br atom is positionally disordered with the carbonyl group in the *trans* position with site occupancies refined to 0.595(2) and its complement. The geometries of the disordered carbonyl groups were restrained to ideal values.

X-ray data refinement for ***4Cl****:* empirical formula $C_{18}H_{13}ClN_5O_3Re$, formula weight 568.98, λ = 0.71073 Å, triclinic, space group $P\bar{1}$, *a* = 6.6905(4) Å, *b* = 10.8368(7) Å, *c* = 13.3444(11) Å, α = 101.192(6)°, β = 90.789(6)°, γ = 98.036(5)°, *V* = 938.96(11) Å^3, *Z* = 2, D_{calcd} = 2.012 Mg/m^3, μ = 6.643 mm^{-1}, crystal size 0.13 × 0.10 × 0.07 mm^3, $2\theta_{max}$ = 55°, 10669 reflections collected, 4308 independent reflections (R_{int} = 0.0539), T_{max}/T_{min} = 0.664/0.517, 4308/0/255 data/restraints/parameters, final *R* indices ($I > 2\sigma(I)$) R1 = 0.0661 and wR2 = 0.1575, *R* indices (all data) R1 = 0.0734, wR2 = 0.1614, largest difference peak and hole 10.633 and −1.768 e/Å^3, CCDC 974871.

X-ray data refinement for ***4Br****:* empirical formula $C_{16}H_{10}BrN_4O_3Re$, formula weight 572.39, λ = 0.71073 Å, triclinic, space group $P\bar{1}$, *a* = 6.7096(14), *b* = 10.825(2), *c* = 12.490(3) Å, α = 68.04(2)°, β = 88.674(19)°, γ = 81.954(16)°, *V* = 832.6(3) Å^3, *Z* = 2, D_{calcd} = 2.283 Mg/m^3, μ = 9.721 mm^{-1}, crystal size 0.35 × 0.14 × 0.03 mm^3, $2\theta_{max}$ = 53°, 5860 reflections collected, 3444 independent reflections (R_{int} = 0.1222), T_{max}/T_{min} = 0.793/0.568, 3444/1/111 data/restraints/parameters, final *R* indices ($I > 2\sigma(I)$) R1 = 0.1267 and wR2 = 0.2083, *R* indices (all data) R1 = 0.1956 and wR2 = 0.2411, largest difference peak and hole 4.951 and −2.888 e/Å^3, CCDC 974872. The data could support anisotropic refinement of the Re and Br atoms only.

X-ray data refinement for ***5Br****:* empirical formula $C_{20}H_{12}BrN_4O_3Re$, formula weight 622.45, λ = 1.54178 Å, monoclinic, space group $P2_1/c$, *a* = 7.1179(9) Å, *b* = 46.0879(5) Å, *c* = 34.7382(5) Å, β = 90.3160(10)°, *V* = 11395.7(15) Å^3, *Z* = 24, D_{calcd} = 2.177 Mg/

dx.doi.org/10.1021/ic403138a | *Inorg. Chem.* 2014, 53, 3629−3641

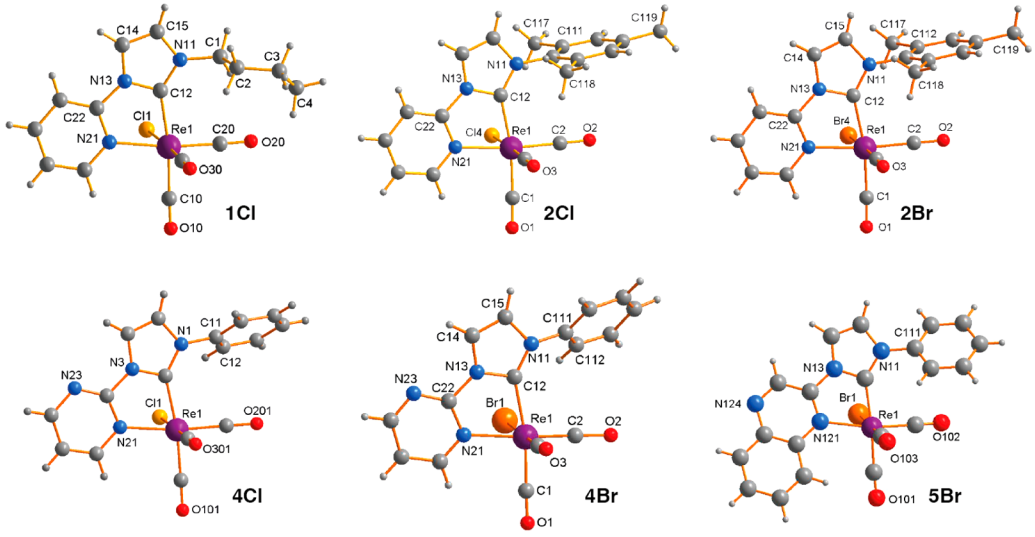

Figure 2. X-ray crystal structures of the complexes **1Cl**, **2Cl**, **2Br**, **4Cl**, **4Br**, and **5Br**.

m^3, μ = 15.250 mm^{-1}, crystal size 0.48 × 0.03 × 0.02 mm^3, $2\theta_{max}$ = 135°, 146805 reflections collected, 20461 independent reflections (R_{int} = 0.0495), T_{max}/T_{min} = 0.762/0.286, 20461/18/1567 data/restraints/parameters, final R indices ($I > 2\sigma(I)$) R1 = 0.0375 and wR2 = 0.0802, R indices (all data) R1 = 0.0412 and wR2 = 0.0817, largest difference peak and hole 1.393 and −0.970 e/Å^{-3}, CCDC 974873.

Computational Calculations. Time-dependent density functional theory (TD-DFT) calculations were performed with GAUSSIAN 09 in order to calculate the absorption spectra for synthesized complexes.[36] Prior to these calculations, the structures were relaxed at the B3LYP level of theory in the presence of an implicit solvent (dichloromethane). The Re atoms were treated with the Stuttgart−Dresden (SDD) effective core potential;[37] the Pople 6-311++G** basis set was used for C, H, N, O, Cl, and Br atoms, and in all calculations the effect of the solvent was mimicked with the PCM solvation model,[38] with parameters adequate for dichloromethane. The low-lying singlet−singlet excitation energies were calculated at the same level of theory, and the spectra were reproduced as the superposition of Gaussian functions with heights proportional to calculated intensities and a variance of 11 nm.

RESULTS AND DISCUSSION

Synthesis and Spectroscopic Characterization of the Complexes. The variously functionalized NHC-based ligands were prepared according to previously published procedures. Aside from a few exceptions, the majority of the complexes were synthesized via a variation of the in situ method developed in our previous work (Figure 1).[14,17] Herein we found that using triethylamine in 10× excess to facilitate the deprotonation of the imidazole C atom, instead of potassium carbonate, afforded in general an improved yield. For the preparation of **1Cl** and **2Cl**, a slight variation of the free carbene method reported by Kaufhold et al. was initially attempted;[31] however, the yields of the isolated products were inferior in comparison to those of the in situ method. **1Cl** could not be synthesized by either the in situ or the free carbene method: therefore, a silver transmetalation approach was utilized, which afforded low to moderate yields. The complex **3Cl** was initially prepared using the in situ method as compared to the silver transmetalation previously attempted by Wang et al.;[16] however, the former was found to produce the complex in low yield. Generally, when synthesizing the bromo complexes *fac*-[Re(CO)$_3$(NHC)Br], the imidazolium salt of the NHC precursor was never used as the chloride to avoid the formation of the targeted complex as a mixture of chloro and bromo species. On the other hand, the synthesis of the chloro complexes *fac*-[Re(CO)$_3$(NHC)Cl] could be performed by starting with any imidazolium salt.

All the complexes display relatively similar peaks in the 2020−1880 cm^{-1} region of their IR spectra, and no significant variation of the frequencies is noted upon changing the R1 and R2 substituents on the NHC ligands (Figure 1). Also, no differences were detected when exchanging the ancillary ligand between chloro and bromo. The lack of variation in the carbonyl peaks indicates that in all cases the electron density of the Re centers remains unaltered, hinting at the fact that any modification of the photophysical behavior of the complexes, in terms of absorption and emission maxima, is likely to be mostly attributed to the NHC π^* acceptor ligand.

The successful synthesis of all complexes was supported, along with the presence of three CO stretching peaks in the IR spectra, by the disappearance of the imidazolium H2 signal in the 10−12 ppm region in the ^{1}H NMR spectra, indicating deprotonation of the NHC precursor. The ^{1}H NMR spectra of **2Cl**, **2Br**, **3Cl**, and **3Br**, bearing the mesityl-substituted NHC ligands, show three separate singlets around 2 ppm, which is consistent with three nonequivalent methyl environments. The presence of these three peaks, instead of two, indicates a restricted rotation of the mesityl unit around the C−N bond, which is likely to originate from the steric hindrance between the *o*-methyl substituents against the adjacent CO ligand and the imidazole H4 atom. On the other hand, the phenyl substituent in **4Cl**, **4Br**, **5Cl**, and **5Br** presents a significantly reduced rotational barrier. The free rotation is in agreement with the fact that in the ^{13}C NMR spectra the phenyl substituents show only four C environments, as opposed to the restricted mesityl rings that show a total of six environments. The ^{13}C NMR spectra of all the complexes display four signals of weak intensity between 199 and 188 nm, corresponding to each of the three individual C atoms of the CO ligands and to the carbene C atom of the imidazole heterocycle.

X-ray Structural Investigation. Single crystals suitable for X-ray diffraction were successfully grown for **1Cl**, **2Cl**, **2Br**, **4Cl**, **4Br**, and **5Br**. The combined structures for these complexes are shown in Figure 2. The facial arrangement of the three carbonyl ligands was confirmed for all species. In all cases, the structures show that the heterocyclic substituent

dx.doi.org/10.1021/ic403138a | Inorg. Chem. 2014, 53, 3629−3641

Table 1. Selected Bond Distances (Å) between the Re Centers and the Three C Atoms of the CO Ligands[a]

Re−CO bond	1Cl	2Cl	2Br	4Cl	5Br
trans to N atom	1.910(3)	1.936(8)	1.921(4)	1.907(10)	1.906(6)
trans to C atom	1.957(2)	1.937(7)	1.952(4)	1.946(10)	1.964(6)
trans to halogen	1.913(3)	1.949(11)	2.002(8)	1.969(14)	2.000(7)

[a]The corresponding values for **4Br** are not reported due to their low precision.

Table 2. Photophysical Properties of the Complexes from Diluted Dichloromethane Solutions (ca. 10^{-5} M)

		emission (room temp)					emission (77 K)	
	absorption λ_{abs} (nm) ($10^4\varepsilon$ (cm^{-1} M^{-1}))	λ_{em} (nm)	τ^a (ns)	τ^b (ns)	Φ^a	Φ^b	λ_{em} (nm)	τ (μs)
1Cl	230 (2.98), 356 (0.56)	514	32	43	0.007[c]	0.012[c]	462	5.7
1Br	230 (2.26), 359 (0.39)	520	9 (73%), 36 (27%)	10 (65%), 48 (35%)	0.006[c]	0.007[c]	464	1.9 (14%), 6.9 (86%,)
2Cl	230 (2.73),, 359 (0.33)	520	50	80	0.008[d]	0.014[d]	470	4.9 (27%), 9.3 (73%)
2Br	230 (3.04), 362 (0.44)	510	19	24	0.001[d]	0.002[d]	470	2.6 (17%), 7.9 (83%)
3Cl[e]	230 (5.09), 362 (0.82)	582	99	300	0.013[d]	0.027[d]	508	10.3
3Br	230 (4.34), 367 (0.61)	577	106	373	0.013[d]	0.033[d]	510	8.5
4Cl	230 (3.81), 364 (0.67)	583	98	211	0.016[d]	0.024[d]	504	7.6
4Br	230 (2.09), 366 (0.32)	575	109	397	0.019[d]	0.060[d]	512	6.0
5Cl	230 (2.62), 344 (0.90), 415(0.36)	494	5	5	0.038[d]	0.052[d]	610	3.6
5Br	230 (3.51), 344 (1.13), 427 (0.41)	432	2	2	<0.001[d]	<0.001[d]	610	5.3

[a]From air-equilibrated solutions. [b]From degassed solutions. [c]Rhodamine 101 in air-equilibrated ethanol used as the reference. [d]$[Ru(bpy)_3]Cl_2$ in air-equilibrated water used as the reference. [e]**3Cl** was previously reported;[16] however, we note slightly different values with respect to the lifetime decay values.

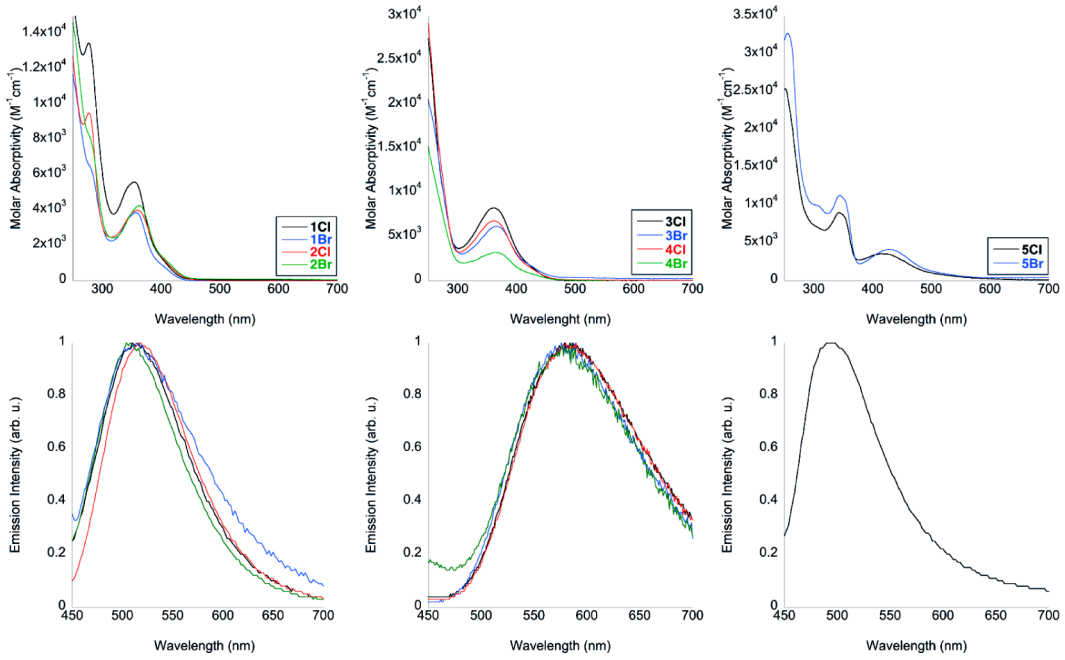

Figure 3. Experimental absorption and emission profiles of the complexes from dilute dichloromethane solutions (ca. 10^{-5} M) at room temperature. The emission profiles were obtained by exciting the complexes to their lowest energy λ_{abs}. The emission profile of **5Br** is not reported due to its extremely weak emission (see the Supporting Information, Figure S11). The same color coding (inset) is used between the absorption and emission profiles of the same group of complexes.

(pyridyl, pyrimidyl, or quinoxyl) is virtually coplanar with the imidazole ring. The mesityl ring in the NHC ligands of **2Cl**, **2Br**, and **3Br** lies almost perpendicular to the imidazole ring, confirming the high degree of steric hindrance that restricts free rotation. In contrast, the phenyl substituent in **4Cl**, **4Br**, and **5Br** is only twisted by ca. 40°. The data suggest that, at least in the solid state, there is limited to no extended π conjugation between the imidazole and the aryl (mesityl or phenyl) rings.

Across the series, the Re−C(NHC) distance is found to be slightly shorter than the Re−N distance, in agreement with the stronger σ donation of the carbene C atom.[26,39] The longest Re−C(NHC) bond belongs to **5Br**, which could be ascribed to the increased steric bulkiness of the quinoxyl-substituted ligand in comparison to the pyridyl- and pyrimidyl-substituted ligands. Notably, despite the stronger *trans* effect attributed to carbene-type ligands (analogously to the corresponding tricarbonyl Re(I) phosphine and phosphite complexes), the longest Re−

dx.doi.org/10.1021/ic403138a | Inorg. Chem. 2014, 53, 3629−3641

CO bond in the complexes appears to be that *trans* to the halogen ligand (Table 1). The only exception is represented by complex **1Cl**. This trend might suggest a diminished *trans* effect from the NHC C atom. On analysis of the pseudo-octahedral geometry around the Re centers, it is in fact noted that the carbene C atom is in each case distorted from its ideal position along the axes of the octahedron. The distortion originates as a consequence of a bite angle lower than 90° from the five-membered ring between the NHC ligands and the Re center; the angles formed between the carbene C atom, the Re atom, and the CO ligand range between 173 and 169°. See the Supporting Information, Tables S1−S6, for complete tables of bond lengths and angles.

Photophysical Investigation. The photophysical data of all the complexes from dilute dichloromethane solutions (ca. 10^{-5} M) are summarized in Table 2, with each absorption and emission profile shown in Figure 3 (see the Supporting Information, Figures S1−S10, for excitation spectra). The absorption spectra display analogous trends, highlighting intense high-energy transitions in the 230−300 nm region followed by red-shifted bands of lower molar absorptivity above 300 nm. The higher energy bands are associated with ligand-centered (LC) $\pi \rightarrow \pi^*$ transitions involving the NHC ligand. In the case of the pyridyl complexes **1Cl**, **1Br**, **2Cl**, and **2Br**, the lower energy band is interpreted as an admixture of MLCT (Re → NHC) and ligand-to-ligand (halogen → NHC; LLCT) charge transfer transitions. The same band assignment was followed in the case of the pyrimidyl complexes **3Cl**, **3Br**, **4Cl**, and **4Br**. Finally, the region above 300 nm in the absorption spectra of **5Cl** and **5Br** shows two bands: the transitions between 300 and 360 nm are assigned to LC transitions, as similar bands appear in the absorption profile of the uncoordinated NHC ligand. On the other hand, the broad band above 360 nm was attributed again to mixed MLCT and LLCT transitions. The lowest energy CT transitions of **5Cl** and **5Br** are red-shifted by ca. 60 nm due to the increased π conjugation when passing from the pyridyl or pyrimidyl to the quinoxyl-substituted NHC ligand.

The nature of the assigned transitions in the absorption spectra was also investigated by means of TD-DFT. The structures of all the complexes were relaxed in dichloromethane and were found to be in good agreement with the structures obtained by means of X-ray diffraction, where the root-mean-square deviation (RMSD) of atomic positions between the crystal structures and the theoretical structures are 0.32 for **5Br** and **4Br**, 3.7 for **1Cl**, and 0.10 for all other complexes. The large deviations for structures **5Br**, **4Br**, and **1Cl** are caused by rotations of the phenyl group or different conformations of the butyl group. If the conformational changes are restricted/ignored, the RMSD of these complexes is reduced to <0.17. In all cases, the major contributors in terms of orbitals to the lower energy transitions are HOMO-1 → LUMO and HOMO → LUMO (see the Supporting Information, Tables S7−S16). An analysis of the contours for these orbitals in each case reveals a contribution to HOMO-1 and HOMO from the 5d orbitals of the Re center and the 3p or 4p orbitals of the chloro or bromo ligands, respectively. A relatively minor contribution to these occupied orbitals is also visible from the CO ligands. On the other hand, the LUMO is mainly composed by the heterocyclic substituent connected to the imidazole ring: pyridyl, pyrimidyl, or quinoxyl. A contribution to the LUMO is also present from the carbene C atom of the imidazole system. These frontier orbitals are illustrated in Figure 4 using the complex **4Cl** as an exemplar (see the Supporting Information, Figures S22−S41, for all other complexes). Overall, the calculations are in agreement with the assigned admixture of MLCT and LLCT character for the lower excited states of the complexes.

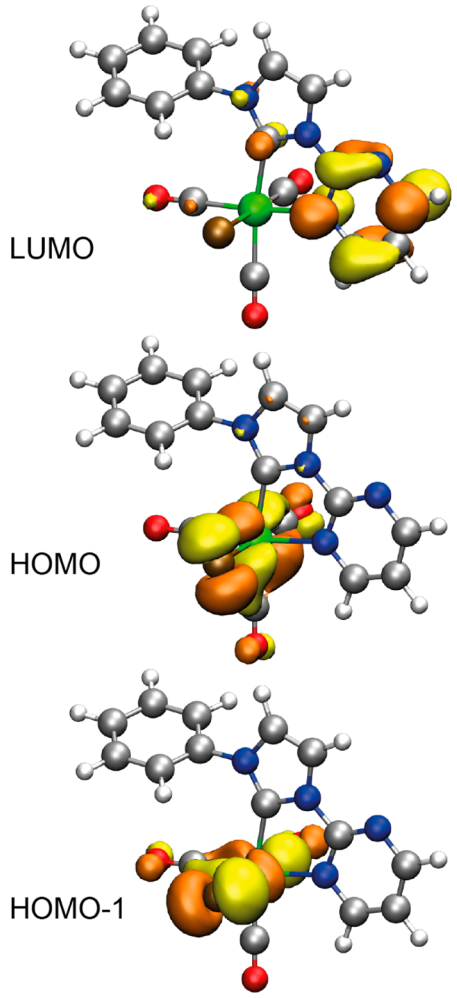

Figure 4. Selected orbital representations for **4Cl**.

The emission profiles of the complexes **1Cl**, **1Br**, **2Cl**, and **2Br** are all very similar and display broad and structureless bands centered at 510−520 nm, typical of emission from excited states of MLCT/LLCT nature (Figure 3). These profiles are also found to be very similar, considering band shape and λ_{em}, to those of previously reported tricarbonyl Re NHC complexes bearing either a benzimidazole ring, instead of an imidazole, or a phenyl substituent directly attached to the imidazole ring, instead of a butyl or mesityl group.[14,17] These similarities confirm that only the pyridine ring strongly influences the nature and energy of the lowest MLCT/LLCT excited state, which is also supported when considering the contours of the LUMO orbital for all the complexes (Figure 4 and Supporting Information, Figures S22−S41). The identical behavior when passing from a butyl to a phenyl or mesityl substituent suggests that very limited conjugation is present between the imidazole and the two aryl rings, as also previously concluded from the X-ray crystal structures. The lifetime decays (τ) of these complexes range between 20 and 80 ns. The complex **1Br** was consistently found to decay following a biexponential fit, a behavior that has been also reported by others for analogous complexes.[15] The τ values seem to

dx.doi.org/10.1021/ic403138a | *Inorg. Chem.* 2014, 53, 3629−3641

elongate on degassing the dichloromethane solutions and the same trend can be observed for the values of quantum yields (Φ). These variations suggest that the emissive state is mainly characterized by a triplet multiplicity (^{3}MLCT/^{3}LLCT).[40,41]

The emission profiles of the pyrimidyl complexes **3Cl**, **3Br**, **4Cl**, and **4Br** appear analogous to those of the pyridyl complexes, although the λ_{em} bands are red-shifted to the 575−583 nm region. While this red shift was less evident from the absorption spectra, it is attributed to the more electron-deficient nature of the pyrimidyl substituent. As in the previous case, the lack of significant variations on passing from the phenyl to the mesityl group on the NHC ligand indicates that the π^* system of the pyrimidyl substituent is the major contributor to the ^{3}MLCT/^{3}LLCT excited state. Again, the elongation of the τ and increase of Φ in degassed solutions suggest the triplet multiplicity of the excited state.[40,41] Notably, the τ values for **3Cl**, **3Br**, **4Cl**, and **4Br** are found to be longer than those of **1Cl**, **1Br**, **2Cl**, and **2Br**, despite the fact that the former group emits from excited states of lower energy, thus contradicting trends dictated by the energy gap law.[42] The shorter lifetime values for the former group might be caused by the competing photochemical pathways triggered upon excitation.

In a frozen matrix at 77 K (see the Supporting Information, Figures S12−S21), all of the complexes bound to the pyridyl- and pyrimidyl-substituted NHC ligands exhibit blue-shifted emission bands as a consequence of the rigidochromic effect.[43] The τ values are found within the 6−10 μs range.

The emission profiles of **5Cl** and **5Br** are found somewhat unusual with respect to the rest of the series. A red-shifted emission would be expected due to the lower energy π^* system of the quinoxyl substituent, as evidenced from the absorption spectra. In fact, this red-shifted emission was previously reported for the analogous quinolyl-NHC complexes.[17] Instead, a blue-shifted band appears in both cases with λ_{em} values at 494 and 432 nm for **5Cl** and **5Br**, respectively, with complex **5Br** characterized by an extremely weak emission (see the Supporting Information, Figure S11). The lifetime decays and quantum yields are very short and virtually insensitive to the presence of O_2. Furthermore, in the case of **5Cl**, the emission profile is found to be very similar to that of the uncoordinated ligand. These data suggest that the emission in both cases might be originating from LC excited states. No emission attributable to a ^{3}MLCT excited state is visible up to 800 nm. Reinforcing these observations is the fact that at 77 K (see the Supporting Information, Figures S20 and S21), both complexes exhibit an intense, broad, and structureless emission profile centered at 610 nm and characterized by τ values of 3.6 and 5.3 μs for **5Cl** and **5Br**, respectively. We attributed this band to the decay from the corresponding ^{3}MLCT/^{3}LLCT states, which appear revived within the frozen matrix, with no contribution from LC states due to suppressed thermal population of higher excited states.

Photochemical Investigation. The photochemical properties of the complexes were investigated by irradiating acetonitrile solutions at 370 nm, following a previously reported procedure,[17] corresponding to excitation to the MLCT/LLCT manifold. The photochemical CO dissociation was initially monitored by means of IR spectroscopy (Figure 5): only the pyridyl complexes **1Cl**, **1Br**, **2Cl**, and **2Br** were found to be photochemically active, whereas the remaining pyrimidyl and quinoxyl complexes were photostable under the same experimental conditions (see the Supporting Information, Figures S42−S53). The three peaks in the 2050−1800 cm^{-1} region, corresponding to the three CO ligands of the starting tricarbonyl complexes (black traces from the spectra in Figure 5), progressively disappear while new peaks at both higher and lower frequencies grow in intensity (red traces from the spectra in Figure 5). The shape of the lower frequency peaks highlights

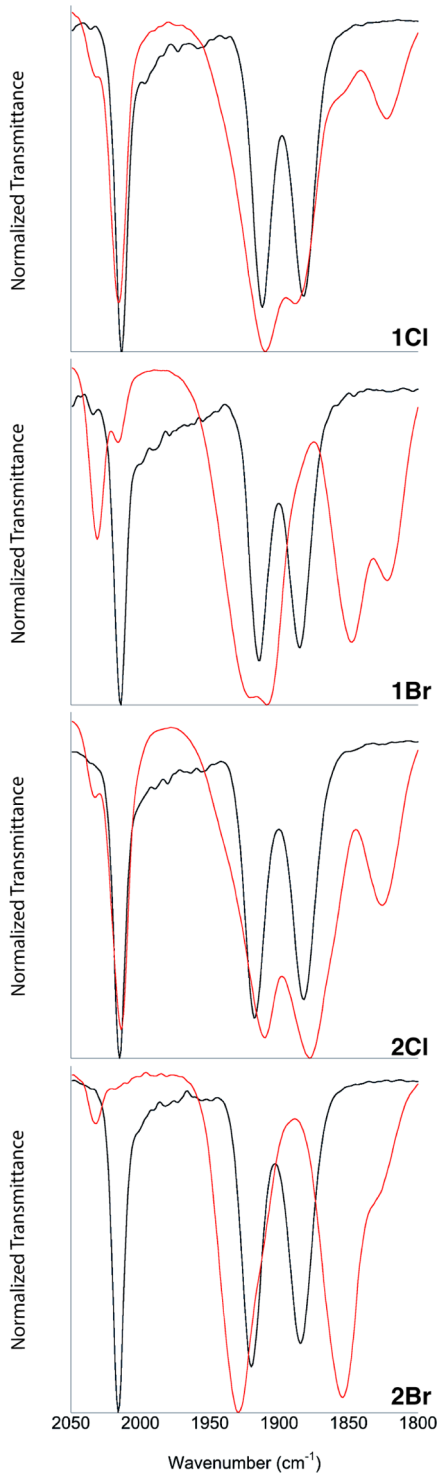

Figure 5. IR progression of the photolysis for **1Cl**, **1Br**, **2Cl**, and **2Br** in acetonitrile solutions. The black traces represent the starting complexes. The photolysis was performed by irradiating each solution at λ 370 nm for 4 h. The products of the photolysis are represented by red traces.

dx.doi.org/10.1021/ic403138a | Inorg. Chem. 2014, 53, 3629−3641

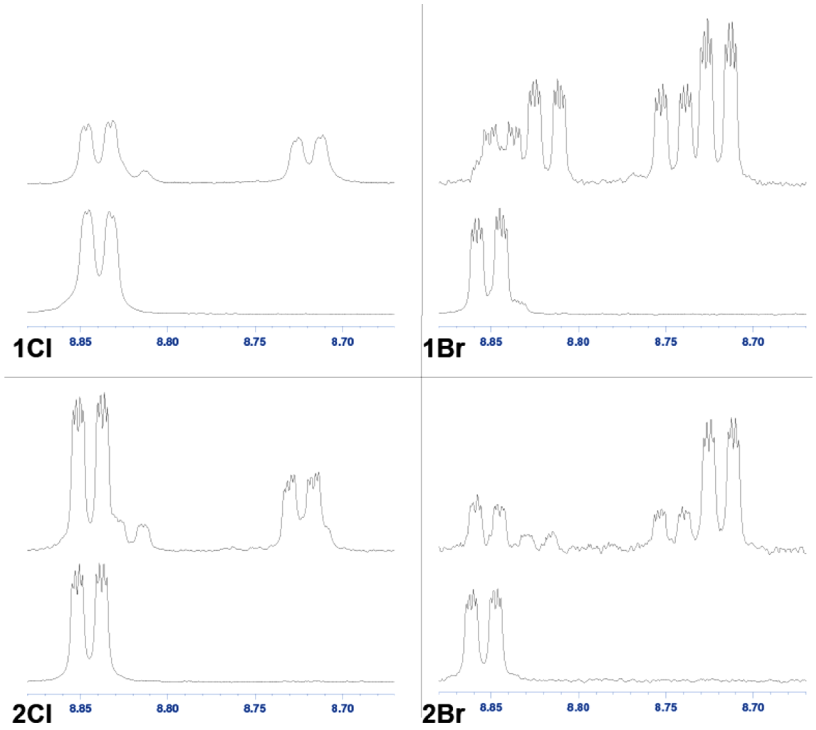

Figure 6. ^{1}H NMR progression of the photolysis for **1Cl**, **1Br**, **2Cl**, and **2Br** in deuterated acetonitrile solutions, obtained by monitoring the pyridyl H6 signal. The photolysis was performed by irradiating each solution at λ 370 nm for 4 h. Initial spectra are reported at the bottom of each panel.

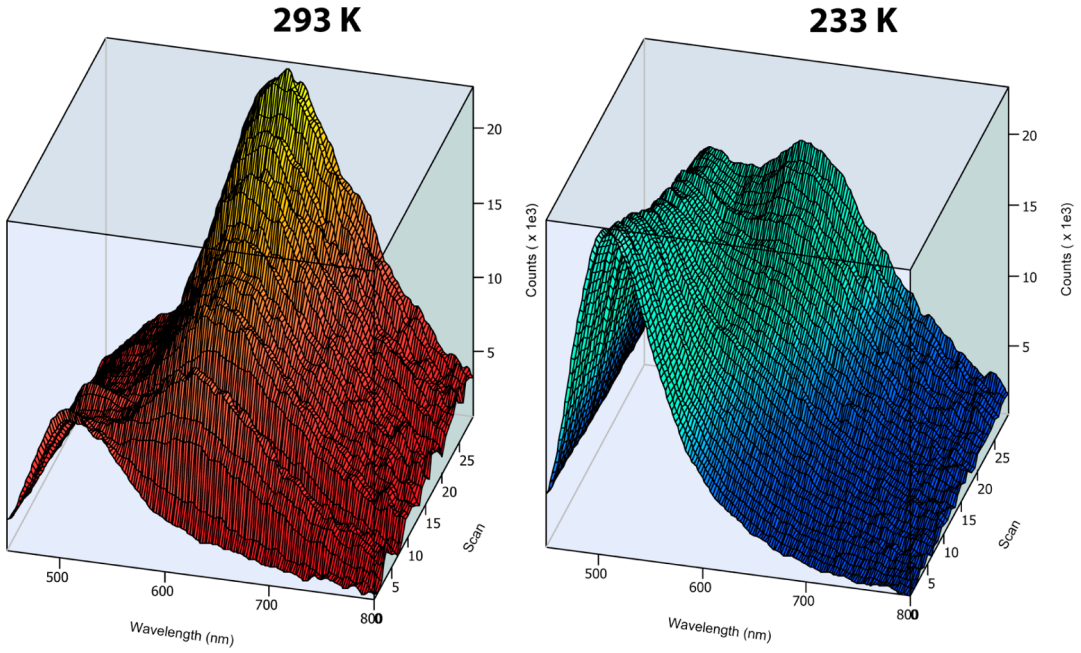

Figure 7. Sequential changes in the emission profiles for a ca. 10^{-5} M degassed acetonitrile solution of **2Br** at 293 and 233 K upon constant excitation at 370 nm.

the presence of two sets each including two individual peaks, which indicates the formation of two distinct dicarbonyl Re complexes. Furthermore, the presence of a higher frequency peak at ca. 2031 cm^{-1} is indicative of the formation of the cationic acetonitrile-solvated complex obtained by ligand exchange of an acetonitrile molecule for the halogen ligand in the starting complexes.[17] The formation of these three products was also confirmed upon monitoring the photolysis in deuterated acetonitrile solutions via ^{1}H NMR spectroscopy (Figure 6). As is more evident in the case of the bromo complexes, the H6 signal at ca. 8.85 ppm of the pyridyl substituent disappears while three distinct new signals arise at ca. 8.83 ppm, corresponding to the tricarbonyl acetonitrile-solvated complex, 8.78, and 8.75 ppm. The last two upfield doublets correspond to the two dicarbonyl complexes, as previously observed.[17]

The combined IR and ^{1}H NMR data highlight the fact that the photolysis of the bromo complexes appears faster than that

dx.doi.org/10.1021/ic403138a | Inorg. Chem. 2014, 53, 3629−3641

of the chloro complexes. Considering that a key intermediate in this bifurcated photochemical pathway seems to be the formation of the tricarbonyl acetonitrile-solvated complex, the fast kinetics of the bromo complexes might be ascribed to the more labile nature of the bromo ligand.

Temperature-dependent photolysis studies were then performed. The shift in the emission profiles of the pyridyl complexes **2Cl** and **2Br**, used as exemplars in a degassed acetonitrile solution at ca. 10^{-5} M, was monitored by recording sequential emission spectra upon constant excitation at 370 nm at temperatures of 293 and 233 K, analogously to the procedure previously reported.[17] Figure 7 shows the three-dimensional plots at both temperatures, highlighting the sequential decrease in intensity of the emission band of **2Br** and the appearance of the characteristic red-shifted band around 590 nm typical of dicarbonyl species (see the Supporting Information, Figures S54 and S55, for **2Cl**). From the spectral sequences in Figure 7, it is evident that the photochemical reaction occurs even at 233 K, although at a significantly slower rate in comparison to the sequence at 293 K. Furthermore, in agreement with the previously discussed IR and NMR data, the photolysis of the bromo complex appears to occur faster than that of the chloro complex. As competing photochemical pathways can act as quenchers for the emissive ^{3}MLCT/^{3}LLCT states,[21] the observed excited state lifetime decays were recorded at various temperatures between 233 and 333 K upon excitation at 375 nm from degassed acetonitrile solutions (ca. 10^{-5} M). The observed decay constant values, k_{obs}, were then plotted as a function of temperature using an Arrhenius-type plot and compared to the k_{obs} data obtained for *fac*-[Re(CO)$_3$(phen)Cl], which is photostable when photolyzed at 370 nm (Figure 8).

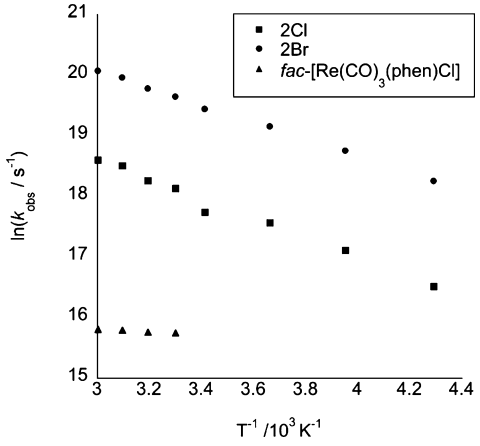

Figure 8. Dependene of ln k_{obs} versus T^{-1} for **2Cl**, **2Br**, and *fac*-[Re(CO)$_3$(phen)Cl]. The corresponding excited-state lifetime decays were recorded upon excitation at 370 nm.

The Arrhenius plot in Figure 8 illustrates that a temperature-dependent nonradiative channel is responsible for the decrease in the excited state lifetime decays of **2Cl** and **2Br** upon an increase in temperature.[44−46] In comparison to the photostable *fac*-[Re(CO)$_3$(phen)Cl], whose dependence of k_{obs} versus T is significantly less pronounced, the trend in **2Cl** and **2Br** might be associated with the presence of photochemically activated transformations. The fact that the photochemistry can be observed at 233 K, however, suggests that the photochemistry might not be occurring from an excited state of LF nature. In fact, these excited states have been shown to reside at quite higher energies for Re tricarbonyl complexes with respect to the CT manifold and,[47−50] in the case of complexes of the type *fac*-[Re(CO)$_3$(diim)(PR$_3$)]$^+$ that undergo CO dissociation from thermally activated ^{3}LF states, the photochemical quantum yield has been shown to rapidly decrease, reaching photostability below 280 K.[21] Furthermore, N-heterocyclic carbene ligands generally act upon increasing the relative energy of LF states via their strong σ donation.[51] On the basis of these observations, it would seem logical to attribute the origin of the photochemical transformations to an excited state of MLCT nature. When the complexes are excited to these states, a decrease in electron density occurs at the Re center and halogen ligand predominantly and, to a minor extent, at the CO ligands. This conclusion is drawn upon considering the orbital contours of the HOMO-1 and HOMO levels. On the other hand, an increase in electron density is localized on the pyridine ring and C atom of the NHC ligand, according to the calculated LUMO levels (Table 3). Therefore, the Re−CO bonds and

Table 3. Calculated Percentage Contribution of the Re, Halogen, and NHC C Atoms to the HOMO-1, HOMO, and LUMO Orbitals

complex	HOMO-1	HOMO	LUMO
1Cl	Re 47; Cl 22	Re 47; Cl 18	C (NHC) 13
1Br	Re 39; Br 37	Re 41; Br 30	C (NHC) 13
2Cl	Re 48; Cl 22	Re 46; Cl 18	C (NHC) 16
2Br	Re 40; Br 35	Re 40; Br 31	C (NHC) 16
3Cl	Re 47; Cl 23	Re 46; Cl 19	C (NHC) 7
3Br	Re 40; Br 37	Re 39; Br 32	C (NHC) 7
4Cl	Re 46; Cl 23	Re 47; Cl 19	C (NHC) 7
4Br	Re 39; Br 37	Re 41; Br 31	C (NHC) 7
5Cl	Re 45; Cl 24	Re 47; Cl 18	C (NHC) 6
5Br	Re 37; Br 39	Re 41; Br 30	C (NHC) 6

Re−X bonds are weakened, while the *trans* effect of the NHC ligand is increased. Whether the photochemical transformation occurs from the lowest (and emissive) MLCT state (LE-MLCT) or from higher energy MLCT states (HE-MLCTs) is still unclear. Furthermore, it cannot be directly concluded whether some photochemical pathways occur directly from the excitation of HE-MLCT upon irradiation at 370 nm or whether the HE-MLCTs are exclusively thermally populated from the LE-MLCT. MLCT states have been previously shown to undergo association of solvent molecules, and the same process might be invoked in this case:[49,52,53] when the complexes are excited to their MLCT states, the association of an acetonitrile molecule might be promoted, thus forming a seven-coordinated intermediate that can eventually result in the dissociation of the halogen ligand and formation of the solvato complex. The dissociation of the CO ligand in a position *trans* to the NHC could occur from the six-coordinated complex in the excited state and/or from the seven-coordinated complex.

The proposed model of the photochemical pathway originating from MLCT-type states can be also used to explain the photostability of the pyrimidyl, quinoxyl, and previously reported quinolyl complexes. In these complexes, the LUMO level might be characterized by a reduced contribution of the C atom of the NHC ligand, as the stabilization of the π^* level of the pyrimidyl, quinolyl, and quinoxyl substituents can act as a "trap" for the electron density in the reduced ligand form of the CT excited state. This trend is also in agreement with the calculated percentage contribution to the LUMO orbital for

dx.doi.org/10.1021/ic403138a | Inorg. Chem. 2014, 53, 3629−3641

these complexes (Table 3). Therefore, the *trans* effect might result in a decrease in the LE-MLCT state and photochemical pathways might be less favored, since the energy gap between the LE-MLCT and the reactive HE-MLCT (where the negative charge is more localized on the carbene C atom, thus increasing its *trans* effect) is increased. However, this rationalization implies that the photochemistry proceeds from thermally activated HE-MLCT states.

In the special case of the quinoxyl complexes **5Cl** and **5Br**, whose emission at room temperature is observed at higher energy (494 and 432 nm, respectively), the lack of photochemistry is ascribed to the $\pi-\pi^*$ LC nature of the excited state. In fact, in this excited state no electron density is significantly withdrawn from the Re, X, or CO ligands; therefore, the Re−CO and Re−X bonds are not weakened and the increase in *trans* effect of the NHC ligand might not be enough to promote photoreactivity.

CONCLUSION

In conclusion, photophysical and photochemical variations in a family of tricarbonyl Re(I) complexes bound to bidentate NHC ligands have been investigated. The photophysical properties of the complexes are found to be almost exclusively dependent on the identity of the heterocyclic substituent bound to the imidazole ring: pyridyl, pyrimidyl, or quinoxyl. The complexes exhibit phosphorescent decay from ^{3}MLCT/^{3}LLCT excited states (aside from an anomalous behavior of the two complexes bound to the quinoxyl NHC ligand), whose relative energy is higher for the pyridyl complexes due to the increased electron deficiency of the pyrimidyl group and extended conjugation of the quinoxyl group. Variations of the other substituent on the imidazole ring among butyl, phenyl, and mesityl did not affect the photophysical properties in any appreciable manner. The pyridyl complexes were found to be photoactive when irradiated to their MLCT/LLCT manifold. In analogy with previously reported complexes, the photochemical reactions resulted in the formation of a tricarbonyl solvato complex along with two distinct dicarbonyl complexes. The photochemistry appears to be faster in the case of the bromo complexes, which was ascribed to the more labile nature of the bromo ligand. Both the pyrimidyl and quinoxyl complexes appear to be photostable. The photochemical studies suggest that the transformations occur from MLCT-type excited states, rendering this photochemical mechanism different from the previously reported CO dissociation from thermally activated ^{3}LF states in *fac*-[Re(CO)$_3$(diim)(PR$_3$)]$^+$ complexes. Overall, the results presented in this paper define the relationship between the chemical nature and photophysical/photochemical properties, including how these can be fine-tuned, of the tricarbonyl Re(I) complexes bound to bidentate NHC imidazole-based ligands.

ASSOCIATED CONTENT

Supporting Information

Tables, figures, and CIF files giving bond lengths and angles for all of the complexes, excitation profiles for all of the complexes at room temperature, excitation and emission profiles for **5Br** at room temperature, excitation and emission profiles for all of the complexes at 77 K, calculated transitions for all of the complexes, pictorial representations of the orbital contours (HOMO-5 to LUMO+5) for all of the complexes, IR and ^{1}H NMR progression for the photostable complexes, and the photochemical progression of **2Cl**. This material is available free of charge via the Internet at http://pubs.acs.org.

AUTHOR INFORMATION

Corresponding Authors

*E-mail for S.S.: stefano.stagni@unibo.it.
*E-mail for M.M.: m.massi@curtin.edu.au.

Notes

The authors declare no competing financial interest.

ACKNOWLEDGMENTS

This work was supported by the Australian Research Council (FT1301000033, FT130100463, and LE1301000052). J.G.V., B.L.R., and P.J.W. thank Curtin University for the Australian Postgraduate Award. The authors acknowledge the facilities and the scientific and technical assistance of the Australian Microscopy & Microanalysis Research Facility at the Centre for Microscopy, Characterisation & Analysis, The University of Western Australia, a facility funded by the University, State and Commonwealth Governments. P.J.W. and P.R. thank the National Computational Infrastructure for the provision of computer time.

REFERENCES

(1) Kirgan, R. A.; Sullivan, B. P.; Rillema, D. P. *Top. Curr. Chem.* **2007**, *281*, 45−100.
(2) Hock, S. J.; Schaper, L.-A.; Herrmann, W. A.; Kühn, F. E. *Chem. Soc. Rev.* **2013**, *42*, 5073−5089.
(3) Coogan, M. P.; Fernández-Moreira, V. *Chem. Commun.* **2013**, *50*, 384−399.
(4) Fernández-Moreira, V.; Thorp-Greenwood, F. L.; Coogan, M. P. *Chem. Commun.* **2010**, *46*, 186−202.
(5) Lo, K.; Hui, W.; Chung, C.; Tsang, K.; Ng, D.; Zhu, N.; Cheung, K. *Coord. Chem. Rev.* **2005**, *249*, 1434−1450.
(6) Mauro, M.; Procopio, E.; Sun, Y.; Chien, C.; Donghi, D.; Panigati, M.; Mercandelli, P.; Mussini, P.; D'Alfonso, G.; De Cola, L. *Adv. Funct. Mater.* **2009**, *19*, 2607−2614.
(7) Yu, T.; Tsang, D. P.-K.; Au, V. K.-M.; Lam, W. H.; Chan, M.-Y.; Yam, V. W.-W. *Chem. Eur. J.* **2013**, *19*, 13418−13427.
(8) Lo, K.; Zhang, K.; Li, S. *Eur. J. Inorg. Chem.* **2011**, *2011*, 3551−3568.
(9) Zou, T.; Lum, C. T.; Chui, S. S.-Y.; Che, C.-M. *Angew. Chem., Int. Ed.* **2013**, *52*, 2930−2933.
(10) Unger, Y.; Zeller, A.; Ahrens, S.; Strassner, T. *Chem. Commun.* **2008**, 3263−3265.
(11) Barbante, G. J.; Francis, P. S.; Hogan, C. F.; Kheradmand, P. R.; Wilson, D. J. D.; Barnard, P. J. *Inorg. Chem.* **2013**, *52*, 7448−7459.
(12) Yang, C.-H.; Beltran, J.; Lemaur, V.; Cornil, J.; Hartmann, D.; Sarfert, W.; Fröhlich, R.; Bizzarri, C.; De Cola, L. *Inorg. Chem.* **2010**, *49*, 9891−9901.
(13) Visbal, R.; Ospino, I.; López-de-Luzuriaga, J. M.; Laguna, A.; Gimeno, M. C. *J. Am. Chem. Soc.* **2013**, *135*, 4712−4715.
(14) Casson, L. A.; Muzzioli, S.; Raiteri, P.; Skelton, B. W.; Stagni, S.; Massi, M.; Brown, D. H. *Dalton Trans.* **2011**, *40*, 11960−11967.
(15) Li, X.-W.; Li, H.-Y.; Wang, G.-F.; Chen, F.; Li, Y.-Z.; Chen, X.-T.; Zheng, Y.-X.; Xue, Z.-L. *Organometallics* **2012**, *31*, 3829−3835.
(16) Wang, G.-F.; Liu, Y.-Z.; Chen, X.-T.; Zheng, Y.-X.; Xue, Z.-L. *Inorg. Chim. Acta* **2013**, *394*, 488−493.
(17) Vaughan, J. G.; Reid, B. L.; Ramchandani, S.; Wright, P. J.; Muzzioli, S.; Skelton, B. W.; Raiteri, P.; Brown, D. H.; Stagni, S.; Massi, M. *Dalton Trans.* **2013**, *42*, 14100−14114.
(18) Ishitani, O.; Kanai, K.; Yamada, Y.; Sakamoto, K. *Chem. Commun.* **2001**, 1514−1515.
(19) Koike, K.; Tanabe, J.; Toyama, S.; Tsubaki, H.; Sakamoto, K.; Westwell, J.; Johnson, F.; Hori, H.; Saitoh, H.; Ishitani, O. *Inorg. Chem.* **2000**, *39*, 2777−2783.

(20) Morimoto, T.; Nishiura, C.; Tanaka, M.; Rohacova, J.; Nakagawa, Y.; Funada, Y.; Koike, K.; Yamamoto, Y.; Shishido, S.; Kojima, T.; Saeki, T.; Ozeki, T.; Ishitani, O. *J. Am. Chem. Soc.* **2013**, *135*, 13266−13269.
(21) Koike, K.; Okoshi, N.; Hori, H.; Takeuchi, K.; Ishitani, O.; Tsubaki, H.; Clark, I.; George, M.; Johnson, F.; Turner, J. *J. Am. Chem. Soc.* **2002**, *124*, 11448−11455.
(22) Ng, C.-O.; Lo, L. T.-L.; Ng, S.-M.; Ko, C.-C.; Zhu, N. *Inorg. Chem.* **2008**, *47*, 7447−7449.
(23) Ko, C.; Lo, L.; Ng, C.; Yiu, S. *Chem. Eur. J.* **2010**, *16*, 13773−13782.
(24) Smithback, J.; Helms, J.; Schutte, E.; Woessner, S.; Sullivan, B. *Inorg. Chem.* **2006**, *45*, 2163−2174.
(25) Pierri, A. E.; Pallaoro, A.; Wu, G.; Ford, P. C. *J. Am. Chem. Soc.* **2012**, *134*, 18197−18200.
(26) Sato, T.; Hirose, Y.; Yoshioka, D.; Oi, S. *Organometallics* **2012**, *31*, 6995−7003.
(27) Gardiner, M. G.; Herrmann, W. A.; Reisinger, C.-P.; Schwarz, J.; Spiegler, M. *J. Organomet. Chem.* **1999**, *572*, 239−247.
(28) Xu, Z.-L.; Li, H.-X.; Ren, Z.-G.; Du, W.-Y.; Xu, W.-C.; Lang, J.-P. *Tetrahedron* **2011**, *67*, 5282−5288.
(29) Loch, J. A.; Albrecht, M.; Peris, E.; Mata, J.; Faller, J. W.; Crabtree, R. H. *Organometallics* **2002**, *21*, 700−706.
(30) Gründemann, S.; Albrecht, M.; Kovacevic, A.; Faller, J. W.; Crabtree, R. H. *Dalton Trans.* **2002**, 2163−2167.
(31) Kaufhold, O.; Hahn, F. E.; Pape, T.; Hepp, A. *J. Organomet. Chem.* **2008**, *693*, 3435−3440.
(32) Demas, J.; Crosby, G. *J. Phys. Chem.* **1971**, *75*, 991−1024.
(33) Eaton, D. *Pure Appl. Chem.* **1988**, *60*, 1107−1114.
(34) Lakowicz, J. R. *Principles of fluorescence spectroscopy*, 3rd ed.; Springer: Baltimore, MD, 2009.
(35) Sheldrick, G. M. *Acta Crystallogr., Sect. A* **2008**, *64*, 112−122.
(36) Frisch, M. J.; Frisch, M. J.; Trucks, G. W.; Schlegel, H. B.; Scuseria, G. E.; Robb, M. A.; Cheeseman, J. R.; Scalmani, G.; Barone, V.; Mennucci, B.; Petersson, G. A.; Nakatsuji, H.; Caricato, M.; Li, X.; Hratchian, H. P.; Izmaylov, A. F.; Bloino, J.; Zheng, G.; Sonnenberg, J. L.; Hada, M.; Ehara, M.; Toyota, K.; Fukuda, R.; Hasegawa, J.; Ishida, M.; Nakajima, T.; Honda, Y.; Kitao, O.; Nakai, H.; Vreven, T.; Montgomery, J. A., Jr.; Peralta, J. E.; Ogliaro, F.; Bearpark, M.; Heyd, J. J.; Brothers, E.; Kudin, K. N.; Staroverov, V. N.; Kobayashi, R.; Normand, J.; Raghavachari, K.; Rendell, A.; Burant, J. C.; Iyengar, S. S.; Tomasi, J.; Cossi, M.; Rega, N.; Millam, J. M.; Klene, M.; Knox, J. E.; Cross, J. B.; Bakken, V.; Adamo, C.; Jaramillo, J.; Gomperts, R.; Stratmann, R. E.; Yazyev, O.; Austin, A. J.; Cammi, R.; Pomelli, C.; Ochterski, J. W.; Martin, R. L.; Morokuma, K.; Zakrzewski, V. G.; Voth, G. A.; Salvador, P.; Dannenberg, J. J.; Dapprich, S.; Daniels, A. D.; Farkas, Ö.; Foresman, J. B.; Ortiz, J. V.; Cioslowski, J.; Fox, D. J. *Gaussian09, Revision B.01*; Gaussian, Inc., Wallingford, CT, 2009.
(37) Andrae, D.; Haeussermann, U.; Dolg, M.; Stoll, H.; Preuss, H. *Theor. Chim. Acta* **1990**, *77*, 123−141.
(38) Tomasi, J.; Mennucci, B.; Cammi, R. *Chem. Rev.* **2005**, *105*, 2999−3094.
(39) Sato, T.; Hirose, Y.; Yoshioka, D.; Shimojo, T.; Oi, S. *Chem. Eur. J.* **2013**, *19*, 15710−15718.
(40) Stagni, S.; Colella, S.; Palazzi, A.; Valenti, G.; Zacchini, S.; Paolucci, F.; Marcaccio, M.; Albuquerque, R. Q.; De Cola, L. *Inorg. Chem.* **2008**, *47*, 10509−10521.
(41) Flamigni, L.; Barbieri, A.; Sabatini, C.; Ventura, B.; Barigelletti, F. *Top. Curr. Chem.* **2007**, *281*, 143−203.
(42) Kober, E.; Caspar, J.; Lumpkin, R.; Meyer, T. *J. Phys. Chem.* **1986**, *90*, 3722−3734.
(43) Xue, W.; Chan, M.; Su, Z.; Cheung, K.; Liu, S.; Che, C. *Organometallics* **1998**, *17*, 1622−1630.
(44) Costa, R. D.; Monti, F.; Accorsi, G.; Barbieri, A.; Bolink, H. J.; Ortí, E.; Armaroli, N. *Inorg. Chem.* **2011**, *50*, 7229−7238.
(45) Schulze, B.; Escudero, D.; Friebe, C.; Siebert, R.; Görls, H.; Sinn, S.; Thomas, M.; Mai, S.; Popp, J.; Dietzek, B.; González, L.; Schubert, U. S. *Chem. Eur. J.* **2012**, *18*, 4010−4025.
(46) Escudero, D.; Heuser, E.; Meier, R. J.; Schäferling, M.; Thiel, W.; Holder, E. *Chem. Eur. J.* **2013**, *19*, 15639−15644.
(47) Vlček, A. *Top. Organomet. Chem.* **2010**, *29*, 73−114.
(48) Vlček, A.; Zális, S. *Coord. Chem. Rev.* **2007**, *251*, 258−287.
(49) Lindsay, E.; Vlcek, A., Jr; Langford, C. H. *Inorg. Chem.* **1993**, *32*, 2269−2275.
(50) Stufkens, D.; Vlček, A. *Coord. Chem. Rev.* **1998**, *177*, 127−179.
(51) Hudson, Z. M.; Sun, C.; Helander, M. G.; Chang, Y.-L.; Lu, Z.-H.; Wang, S. *J. Am. Chem. Soc.* **2012**, *134*, 13930−13933.
(52) Sato, S.; Matubara, Y.; Koike, K.; Falkenström, M.; Katayama, T.; Ishibashi, Y.; Miyasaka, H.; Taniguchi, S.; Chosrowjan, H.; Mataga, N.; Fukazawa, N.; Koshihara, S.; Onda, K.; Ishitani, O. *Chem. Eur. J.* **2012**, *18*, 15722−15734.
(53) Sato, S.; Sekine, A.; Ohashi, Y.; Ishitani, O.; Blanco-Rodríguez, A. M.; Vlček, A.; Unno, T.; Koike, K. *Inorg. Chem.* **2007**, *46*, 3531−3540.